

ADAPTIVE EXPONENTIAL INTEGRATION FOR STABLE GAUSSIAN MIXTURE BLACK-BOX VARIATIONAL INFERENCE*

BAOJUN CHE[†], YIFAN CHEN[‡], DANIEL ZHENGYU HUANG[§], XINYING MAO[†], AND
WEIJIE WANG[†]

Abstract. Black-box variational inference (BBVI) with Gaussian mixture families offers a flexible approach for approximating complex posterior distributions without requiring gradients of the target density. However, standard numerical optimization methods often suffer from instability and inefficiency. We develop a stable and efficient framework that combines three key components: (1) affine-invariant preconditioning via natural gradient formulations, (2) an exponential integrator that unconditionally preserves the positive definiteness of covariance matrices, and (3) adaptive time stepping to ensure stability and to accommodate distinct warm-up and convergence phases. The proposed approach has natural connections to manifold optimization and mirror descent. For Gaussian posteriors, we prove exponential convergence in the noise-free setting and almost-sure convergence under Monte Carlo estimation, rigorously justifying the necessity of adaptive time stepping. Numerical experiments on multimodal distributions, Neal’s multiscale funnel, and a PDE-based Bayesian inverse problem for Darcy flow demonstrate the effectiveness of the proposed method.

Key words. Variational Inference, Adaptive Exponential Integration, Natural Gradient, Gaussian Mixture, Gradient Free

MSC codes. 62F15, 65M32, 65L20, 90C56

1. Introduction. Sampling from probability distributions known only up to a normalization constant is a central task in Bayesian inference and uncertainty quantification for scientific computing. Consider a target distribution with density

$$(1.1) \quad \pi(\theta) \propto e^{-\Phi_R(\theta)},$$

where $\Phi_R(\theta)$ denotes a known potential function. The objective is to efficiently generate samples from π or to compute expectations with respect to it. In large-scale Bayesian inverse problems [37, 56, 47, 7, 55, 19, 58, 9, 26, 29], evaluating Φ_R typically requires computationally expensive forward model simulations, rendering traditional sampling approaches such as Markov chain Monte Carlo (MCMC) methods prohibitively costly.

Variational inference [35, 6, 14] provides a powerful alternative by reformulating sampling as an optimization problem. Rather than drawing samples directly from π , one introduces a tractable parametric family of distributions $\{\rho_a\}$, indexed by parameters a , and seeks the member that is closest to π in the sense of the Kullback–Leibler (KL) divergence:

$$(1.2) \quad \min_{\rho_a} \text{KL}[\rho_a \| \pi] = \int \rho_a \log \rho_a \, d\theta + \int \rho_a \Phi_R \, d\theta + \text{const.}$$

*Submitted to the editors DATE. The authors are in alphabetical order.

Funding: B. Che, D.Z. Huang, X. Mao, and W. Wang acknowledge funding support from National Key R&D Program of China 2025YFA1018700, National Natural Science Foundation of China (No.12471403, 62595771, and 12288101) and the Fundamental Research Funds for the Central Universities of China.

[†]School of Mathematical Sciences, Peking University, Beijing, China
(bjche25@stu.pku.edu.cn, maoxinying@stu.pku.edu.cn, wwj66285509350@stu.pku.edu.cn).

[‡]Department of Mathematics, University of California, Los Angeles, CA, USA (yifanfchen@math.ucla.edu)

[§]Corresponding author. Beijing International Center for Mathematical Research, Center for Machine Learning Research, Peking University, Beijing, China (huangdz@bicmr.pku.edu.cn).

This optimization-based viewpoint enables efficient approximations in settings where exact sampling is infeasible but accurate approximations are sufficient. Indeed, it underpins many classical approaches in Bayesian inference and inverse problems, including methods based on Gaussian approximations [48, 32, 39], Kalman-filter-type methods [38, 36, 21, 47, 2, 33, 12, 42], and mean-field approaches [34, 35, 18].

Despite their success, Gaussian approximations are often inadequate for posteriors that are multimodal, multiscale, or exhibit complex geometric structure. To address these limitations, more expressive variational families have been developed, including Gaussian mixture models [34] and normalizing flows [52]. In particular, Gaussian mixture models offer great flexibility while retaining computational tractability [24, 3].

In many contemporary applications, the potential Φ_R is accessible only as a black box [51], with derivatives with respect to θ either unavailable or unreliable. This setting motivates black-box variational inference (BBVI) methods [51, 28, 20], which avoid direct use of $\nabla\Phi_R$. Instead, BBVI relies on the log-derivative (score-function) identity combined with Monte Carlo integration to approximate gradients of the form $\nabla_a \text{KL}[\rho_a \| \pi]$; see details in [subsection 1.2.2](#). Alternative gradient-free approaches approximate these integrals using specialized high-dimensional quadrature rules, often motivated by ensemble Kalman filter and unscented transform methodologies [17, 13]. While such methods can be effective in certain regimes, BBVI remains particularly attractive due to its simplicity, general applicability, and unbiased gradient estimation, which are the focus of the present work.

Nevertheless, Gaussian mixture BBVI methods can encounter serious numerical challenges. In particular, covariance matrices may lose positive definiteness during optimization. These difficulties are further exacerbated by Monte Carlo noise in the gradient estimators—especially in high-dimensional settings—and by sensitivity to initialization, which together can lead to slow convergence or even optimization failure [3, 51].

In this paper, we address these stability and efficiency challenges by combining affine-invariant natural gradient formulations with a new adaptive exponential integration scheme and rigorous theoretical analysis. These developments establish Gaussian mixture BBVI as a simple, efficient, and robust framework for gradient-free Bayesian inference.

1.1. Contributions. The primary objective of this work is to develop efficient, stable, and gradient-free numerical schemes for continuous affine-invariant natural gradient flows used as an optimization strategy in Gaussian mixture BBVI. Our main contributions are as follows:

1. We propose a novel exponential integrator with adaptive time stepping for Gaussian mixture BBVI. The method unconditionally preserves the positive definiteness of covariance matrices throughout the evolution, and admits connections to manifold optimization and mirror descent.
2. We provide a rigorous convergence analysis of the proposed scheme in the Gaussian setting. In particular, we establish exponential convergence in the absence of Monte Carlo integration noise and prove convergence under a decaying step-size scheduler when stochastic noise is present. These results justify the use of adaptive time stepping and clarify the roles of distinct warm-up and convergence phases in the algorithm, including its ability to efficiently mitigate the effects of poor initialization during the warm-up phase.
3. We demonstrate the practical effectiveness of the proposed method on a range of challenging numerical examples, including multimodal target distributions,

Neal’s multiscale funnel, and a Bayesian inverse problem for Darcy flow.

1.2. Preliminaries and literature review.

1.2.1. Natural gradient. Conventional gradient descent exhibits a fundamental dependence on the chosen parameterization of the model, which can lead to severe ill-conditioning and the need for very small step sizes, particularly when optimization is performed on curved statistical manifolds. This limitation arises because the standard gradient corresponds to the direction of steepest descent with respect to the Euclidean metric on the parameter space, without accounting for the intrinsic geometry of the family of probability distributions.

Natural gradient methods [1, 44, 11] address this issue by preconditioning the gradient using the Riemannian metric induced by the statistical manifold. This metric is given by the Fisher information matrix (FIM), which captures the local curvature of the model:

$$\frac{da}{dt} = -\text{FIM}(a)^{-1} \nabla_a \text{KL}[\rho_a \parallel \pi], \quad \text{FIM}(a) := \int (\nabla_a \log \rho_a(\theta)) (\nabla_a \log \rho_a(\theta))^T \rho_a(\theta) d\theta.$$

Natural gradient flows are invariant under smooth reparameterizations and ensure that the resulting optimization trajectory depends only on the geometry of the distribution space. We further highlight their affine invariance [25, 16] with respect to linear transformations of the parameter space in the Gaussian and mixture context, which is the key to robustness to anisotropy and ill-conditioning (see Section 3).

Natural gradients have been widely used to accelerate Gaussian variational inference [1, 48, 30, 23, 16], since the Fisher information matrix admits a closed-form expression for Gaussian families. Extending this framework to Gaussian mixture models is considerably more challenging due to parameter coupling and degeneracies in the Fisher matrix. Early approaches relied on block-diagonal or approximate Fisher information matrices to retain tractability [3]. More recently, carefully designed approximations have been shown to significantly improve convergence and robustness for Gaussian mixture variational inference [41], including in gradient-free settings [13].

1.2.2. Black-box variational inference. Many variational inference methods rely on first- or second-order derivative information of the potential Φ_R [5, 6], which may be unavailable or unreliable when Φ_R is accessible only through a black-box forward model. Black-box variational inference (BBVI) [51] was introduced to overcome this limitation by constructing unbiased Monte Carlo estimates of the gradient of the KL divergence.

Specifically, BBVI employs the score-function (log-derivative) identity to rewrite the gradient of the KL divergence with respect to the variational parameters a as

$$(1.3) \quad \nabla_a \text{KL}[\rho_a \parallel \pi] = \mathbb{E}_{\rho_a} [\nabla_a \log \rho_a(\theta) (\log \rho_a(\theta) + \Phi_R(\theta))].$$

The expectation in (1.3) is approximated using Monte Carlo sampling, yielding an unbiased stochastic gradient estimator that does not require derivatives of Φ_R .

In its standard formulation, BBVI combines this Monte Carlo gradient estimator with stochastic gradient descent in the Euclidean parameter space. While broadly applicable, this approach can suffer from high variance in the gradient estimator, sensitivity to step-size selection, and dependence on parameterization, particularly in high-dimensional settings or when expressive variational families such as Gaussian mixtures are employed. These challenges have motivated extensive work on variance reduction and stabilization techniques [51, 49, 57].

The conditioning issues inherent to Euclidean stochastic optimization in BBVI motivate the use of affine-invariant methods such as natural gradients. However, although natural gradients can alleviate some of the conditioning issues inherent to Euclidean BBVI, their application to Gaussian mixture models results in complex continuous-time dynamics for which stable and efficient numerical discretization is nontrivial. We need carefully designed integration schemes to stabilize the algorithm. Addressing these challenges is the primary focus of the present work.

1.3. Organization. In section 2, we introduce natural gradients for the Gaussian mixture family, and propose an exponential integrator with adaptive time stepping for its discretization, forming the basis of our BBVI method. Section 3 provides theoretical insights behind the proposed algorithm, including its convergence, connections to manifold optimization, and affine invariance. Section 4 presents several implementation details, such as scheduler and annealing-based initialization. Numerical experiments are described in section 5, which demonstrate the effectiveness of the proposed framework for Bayesian inference. Finally, concluding remarks are provided in section 6.

2. Stable Gaussian mixture BBVI. In this section, we first formulate the natural gradient flow for Gaussian mixture variational inference. We then introduce an adaptive time integration scheme for its stable discretization, which constitutes our main algorithm.

We consider a Gaussian mixture variational family

$$\rho_a^{\text{GM}}(\theta) = \sum_{k=1}^K w_k \mathcal{N}(\theta; m_k, C_k), \quad a := [m_1, \dots, m_K, C_1, \dots, C_K, w_1, \dots, w_K],$$

where K denotes the number of mixture components. The distribution is parameterized by component means $m_k \in \mathbb{R}^{N_\theta}$, covariance matrices $C_k \in \mathbb{R}^{N_\theta \times N_\theta}$, and nonnegative weights $w_k \in \mathbb{R}_{\geq 0}$ satisfying $\sum_{k=1}^K w_k = 1$. These parameters are collected into the vector a .

2.1. Natural gradient variational inference. Natural gradient methods are widely used in variational inference due to their ability to accelerate optimization by incorporating local geometric information through the Fisher information matrix. However, for Gaussian mixture models, the Fisher information matrix does not admit a closed-form expression. Moreover, the full matrix has dimension $K(N_\theta^2 + N_\theta + 1) \times K(N_\theta^2 + N_\theta + 1)$, making direct inversion computationally prohibitive.

In practice, the Fisher information matrix is often approximated by a block-diagonal matrix [17, Appendix C.8] [41, 13]. This approximation leads to the following natural gradient flow for each mixture component $k = 1, \dots, K$:

$$\begin{aligned} \frac{dm_k}{dt} &= -C_k \int \mathcal{N}_k(\theta) \left(\nabla_\theta \log \rho_a^{\text{GM}} + \nabla_\theta \Phi_R \right) d\theta \\ &= -\mathbb{E}_{\mathcal{N}_k} \left[\theta \left(\log \rho_a^{\text{GM}} + \Phi_R - \mathbb{E}_{\mathcal{N}_k} [\log \rho_a^{\text{GM}} + \Phi_R] \right) \right], \\ (2.1) \quad \frac{dC_k}{dt} &= -C_k \int \mathcal{N}_k(\theta) \left(\nabla_\theta \nabla_\theta \log \rho_a^{\text{GM}} + \nabla_\theta \nabla_\theta \Phi_R \right) d\theta C_k \\ &= -\mathbb{E}_{\mathcal{N}_k} \left[(\theta - m_k)(\theta - m_k)^T \left(\log \rho_a^{\text{GM}} + \Phi_R - \mathbb{E}_{\mathcal{N}_k} [\log \rho_a^{\text{GM}} + \Phi_R] \right) \right], \\ \frac{d \log w_k}{dt} &= - \int \left(\mathcal{N}_k(\theta) - \rho_a^{\text{GM}} \right) \left(\log \rho_a^{\text{GM}} + \Phi_R \right) d\theta. \end{aligned}$$

Here, $\mathcal{N}_k = \mathcal{N}(\theta; m_k, C_k)$ denotes the k -th Gaussian component, and all quantities depend implicitly on time t . Expectations are taken with respect to \mathcal{N}_k .

The above formula that does not involve derivatives of Φ_R is obtained by applying integration by parts. Following the “sticking-the-landing” principle [54], the resulting expressions ensure that the variance of the stochastic estimators of the gradients vanishes as ρ_a^{GM} approaches the target density, i.e., when $\log \rho_a^{\text{GM}} + \Phi_R \approx 0$, enabling low-variance Monte Carlo approximations near convergence. Moreover, the natural gradient flow involves only matrix operations of size $N_\theta \times N_\theta$, making the method computationally feasible for moderate-dimensional problems.

In the next subsection, we present our main contribution: a stable and practical time discretization of the natural gradient flow.

2.2. Adaptive exponential integration. To construct a stable scheme, we reparameterize the covariance matrices using a square-root factorization (e.g., the Cholesky decomposition),

$$C_k = L_k L_k^T.$$

We further define

$$(2.2) \quad f_k(t, \theta) = \log \rho_{a(t)}^{\text{GM}}(L_k(t)\theta + m_k(t)) + \Phi_R(L_k(t)\theta + m_k(t)).$$

Under this reparameterization, expectations with respect to \mathcal{N}_k can be expressed in terms of the standard Gaussian distribution $\mathcal{N} = \mathcal{N}(0, I)$. More precisely, substituting (2.2) into (2.1) yields

$$(2.3a) \quad \frac{dm_k}{dt} = -L_k \mathbb{E}_{\mathcal{N}}[\theta(f_k - \mathbb{E}_{\mathcal{N}}[f_k])],$$

$$(2.3b) \quad \frac{dC_k}{dt} = -L_k \mathbb{E}_{\mathcal{N}}[\theta \theta^T (f_k - \mathbb{E}_{\mathcal{N}}[f_k])] L_k^T,$$

$$(2.3c) \quad \frac{d \log w_k}{dt} = -\mathbb{E}_{\mathcal{N}}[f_k] + \sum_{i=1}^K w_i \mathbb{E}_{\mathcal{N}}[f_i].$$

A key difficulty in time integration is that, for large step sizes, the covariance update may lose positive definiteness [13, Section 3]. To address this issue, we define

$$(2.4) \quad E_k(t) = \mathbb{E}_{\mathcal{N}}[\theta \theta^T (f_k(t, \theta) - \mathbb{E}_{\mathcal{N}}[f_k(t, \theta)])]$$

and employ an exponential-type integrator for the covariance update (2.3b):

$$(2.5) \quad C_k(t_n + \Delta t_n) = L_k(t_n) e^{-E_k(t_n) \Delta t_n} L_k(t_n)^T,$$

This update is independent of the particular square-root factorization. Indeed, for any alternative factorization $L'_k(t_n) = L_k(t_n)Q$ with orthogonal Q , the corresponding matrix $E'_k(t_n) = Q^T E_k(t_n)Q$ yields the same covariance update (2.5). We emphasize that this update unconditionally preserves the positive definiteness of the covariance matrix.

The mean and weight updates are computed using a forward Euler step:

$$(2.6) \quad \begin{aligned} m_k(t_n + \Delta t) &= m_k(t_n) - \Delta t_n L_k(t_n) \mathbb{E}_{\mathcal{N}}[\theta(f_k(t_n, \theta) - \mathbb{E}_{\mathcal{N}}[f_k(t_n, \theta)])], \\ \log w_k(t_n + \Delta t) &= \log w_k(t_n) - \Delta t_n \left(\mathbb{E}_{\mathcal{N}}[f_k(t_n, \theta)] - \sum_i w_i \mathbb{E}_{\mathcal{N}}[f_i(t_n, \theta)] \right). \end{aligned}$$

All expectations in (2.4) and (2.3) are approximated using Monte Carlo sampling, as is standard in BBVI. For each component k , we draw J samples $\{\theta_k^j\}_{j=1}^J \sim \mathcal{N}(0, I)$ and use them to estimate $\mathbb{E}_{\mathcal{N}}[f_k]$ and the corresponding centered moments $\mathbb{E}_{\mathcal{N}}[\theta f_k]$ and $\mathbb{E}_{\mathcal{N}}[\theta \theta^T f_k]$. This procedure requires JK evaluations of Φ_R per time step.

Finally, the time step Δt_n is selected adaptively:

$$(2.7) \quad \Delta t_n = \min \left\{ \Delta t_{\max} \eta(t_n), \frac{\beta}{\max_k \|E_k(t_n)\|_2} \right\},$$

where Δt_{\max} is a prescribed maximum step size, β is a stability parameter, and $\eta(t)$ is a scheduling function that decays from 1 to a small value to mitigate Monte Carlo noise. $E_k(t_n)$ is also estimated using Monte Carlo (using the formula (2.4)). A detailed discussion of this adaptive time-stepping strategy is provided in [subsection 3.1](#).

3. Theoretical insights. In this section, we study the aforementioned variational inference algorithm from two perspectives. In [subsection 3.1](#), we analyze its convergence at the discrete level, showing that adaptive time-stepping is required to guide the transition from the warm-up phase to the convergence phase, and that the scheduler plays an important role in controlling the noise. In [subsection 3.2](#), we present a complementary manifold optimization perspective, which connects the aforementioned algorithm with mirror descent and helps explain its covariance properties, weight positivity, and affine invariance.

3.1. Convergence study. In this subsection, we study the convergence properties of the aforementioned algorithm at the discrete level for the Gaussian case, i.e., $\Phi_R(\theta) = \frac{1}{2}(\theta - m_{\star})^T C_{\star}^{-1}(\theta - m_{\star})$, with mode number $K = 1$. Let

$$(3.1) \quad \Sigma_n = C_{\star}^{-\frac{1}{2}} C(t_n) C_{\star}^{-\frac{1}{2}} \quad \text{and} \quad v_n = C_{\star}^{-\frac{1}{2}} (m(t_n) - m_{\star}),$$

and assume the integral terms (2.3) are computed exactly (whereas in practice, they are typically evaluated by Monte Carlo, with noise). The updates of the mean and covariance in (2.5) and (2.6) then take the form

$$(3.2) \quad v_{n+1} = (I - \Delta t_n \Sigma_n) v_n, \quad \Sigma_{n+1} = L_n e^{\Delta t_n (-L_n^T L_n + I)} L_n^T = h_n(\Sigma_n),$$

where

$$(3.3) \quad L_n = C_{\star}^{-\frac{1}{2}} L(t_n) \quad \text{and} \quad h_n(x) = x e^{\Delta t_n (1-x)}.$$

The derivation can be found in [section A](#). For the noise-free case, we fix the scheduler $\eta(t) = 1$ and do not need to decrease it. The time-step size Δt_n defined in (2.7) then becomes

$$(3.4) \quad \Delta t_n = \min \left\{ \Delta t_{\max}, \frac{\beta}{\|\Sigma_n - I\|_2} \right\}.$$

Here we used the fact $\|E_k(t_n)\|_2 = \|I - L_n^T L_n\|_2 = \|\Sigma_n - I\|_2$. With this adaptive time-stepping, we show in the following theorem that the iteration (3.2) converges exponentially fast (i.e., $\Sigma_n \rightarrow I$ and $v_n \rightarrow 0$) and exhibits only logarithmic dependence on the norm of its initial condition Σ_0 and v_0 . This result is consistent with the continuous-level convergence analysis in [16, Theorem 5.6] and related works [22, 10, 8, 15], where the error decays as $\mathcal{O}(e^{-t})$, with hidden constants depending on the initial condition and the solution. The proof is deferred to [Section A](#).

THEOREM 3.1. *Assume that $\Delta t_{\max} \leq 1$, $\beta \leq 1$, and that the initial covariance matrix Σ_0 is symmetric positive definite with minimum and maximum eigenvalues $\lambda_{\min}(\Sigma_0)$ and $\lambda_{\max}(\Sigma_0)$. Given an error tolerance $\epsilon < 1$, for iterations (3.2) with the adaptive time-stepping (3.4), there exists $N = \mathcal{O}(|\ln \lambda_{\min}(\Sigma_0)| + |\ln \lambda_{\max}(\Sigma_0)| + \max\{\ln \|v_0\|_2, 0\} + \ln \frac{1}{\epsilon})$, such that for all $n > N$,*

$$(3.5) \quad \|\Sigma_n - I\|_2 \leq \epsilon, \quad \|v_n\|_2 \leq \epsilon,$$

where the hidden constant in the $\mathcal{O}(\cdot)$ depends only on Δt_{\max} and β .

Remark 3.2. The convergence behavior proceeds in two phases. In the warm-up phase, all eigenvalues of Σ_n approach 1 within a neighborhood of size independent of Σ_0 after $\mathcal{O}(|\ln \lambda_{\min}(\Sigma_0)| + |\ln \lambda_{\max}(\Sigma_0)|)$ iterations. The adaptive time step $\frac{\beta}{\|\Sigma_n - I\|_2}$ ensures exponential convergence to this neighborhood while preventing numerical instability. This is followed by the convergence phase, in which Σ_n converges to I with error at most ϵ in $\mathcal{O}(\ln \frac{1}{\epsilon})$ iterations. Meanwhile, the iteration for v_n yields a contraction mapping due to the adaptive time-stepping in (3.4), which guarantees a contraction factor strictly less than one. Consequently, v_n converges to 0 within $\mathcal{O}(\ln \|v_0\|_2 + \ln \frac{1}{\epsilon})$ iterations. \diamond

Remark 3.3. When only a single term in (3.4) is used, numerical instability or loss of exponential convergence can occur. For example, if only Δt_{\max} is used, then for large initial condition (in the warm-up phase), the first iteration yields

$$\Sigma_1 = \Sigma_0 e^{-\Delta t_{\max}(\Sigma_0 - 1)},$$

which remains positive but becomes exponentially small. Conversely, if only $\frac{\beta}{\|\Sigma_n - I\|_2}$ is used, then Σ_n oscillates around I in the convergence phase. Specifically, when $\Sigma_n \in (e^{-\beta/2}, e^{\beta/2})$, one finds $\Sigma_{n+1} \notin (e^{-\beta/2}, e^{\beta/2})$. \diamond

Next, we consider the effect of the scheduler in the presence of noise. When the integral terms in (2.4) and (2.6) are estimated via the Monte Carlo method, stochastic errors are introduced. We write the estimated integrals under errors as

$$\mathbb{E}_{\mathcal{N}}[\theta\theta^T(f - \mathbb{E}_{\mathcal{N}}[f])] = \mathbf{L}_n^T \mathbf{L}_n - I - \Omega_n \quad \text{and} \quad \mathbb{E}_{\mathcal{N}}[\theta(f - \mathbb{E}_{\mathcal{N}}[f])] = \mathbf{L}_n^T v_n + \tilde{w}_n,$$

where \mathbf{L}_n defined in (3.3) is a square root of Σ_n satisfying $\Sigma_n = \mathbf{L}_n \mathbf{L}_n^T$. The terms Ω_n and \tilde{w}_n denote the stochastic errors in the covariance and mean updates at the n -th iteration arising from the Monte Carlo approximations. Accordingly, the updates of the mean and covariance, in place of (3.2), are given by

$$(3.6) \quad v_{n+1} = v_n - \Delta t_n (\mathbf{L}_n (\mathbf{L}_n^T v_n + \tilde{w}_n)) \quad \text{and} \quad \Sigma_{n+1} = \mathbf{L}_n e^{\Delta t_n (-\mathbf{L}_n^T \mathbf{L}_n + I + \Omega_n)} \mathbf{L}_n^T.$$

In the stochastic setting, we primarily demonstrate that when Gaussian variational inference has reached a certain accuracy level, an appropriately decaying scheduler selection can guarantee the convergence.

Assumption 1. For all $n \geq 1$, we make the following assumptions:

1. $\sigma(\Sigma_n), \|v_n\|_2 < C_0$, with some $C_0 > 1$.
2. The zero mean Monte Carlo approximation noise for the covariance and mean updates are Ω_n and \tilde{w}_n , where Ω_n is a symmetric noise matrix.

The time step in (2.7) is given by $\Delta t_n = \min\{\eta(t_n)\Delta t_{\max}, \frac{\beta}{\|-\mathbf{L}_n^T \mathbf{L}_n + I + \Omega_n\|_2}\}$, which depends on both Σ_n and Ω_n . Under the above assumptions, we have the following convergence guarantee. The proof can be found in [section A](#).

THEOREM 3.4. *Under Assumption 1, the update scheme given by (3.6) with the time step $\Delta t_n = \min\{\eta(t_n)\Delta t_{\max}, \frac{\beta}{\|-\mathbf{L}_n^T \mathbf{L}_n + I + \Omega_n\|_2}\}$, where $\sum_n \eta(t_n) = +\infty$ and $\sum_n \eta(t_n)^2 < +\infty$, ensures the almost sure convergence of Σ_n to the identity matrix I and v_n to 0.*

3.2. Relation to manifold optimization and mirror descent. In this subsection, we study the aforementioned algorithm from a manifold optimization perspective, showing that it is naturally designed within the framework of mirror descent [4] to ensure positivity and affine invariance.

The covariance update in (2.5) can be interpreted as a matrix optimization problem constrained to the Riemannian manifold of symmetric positive definite (SPD) matrices \mathcal{S}_{++} . On this manifold, the tangent space at a point $X \in \mathcal{S}_{++}$, denoted $T_X \mathcal{S}_{++}$, consists of symmetric matrices. The affine invariant Riemannian metric and distance are defined as [50, 27]

$$g_X(\sigma_1, \sigma_2) = \text{tr}(X^{-1} \sigma_1 X^{-1} \sigma_2), \quad d(X, Y) = \|\log(X^{-\frac{1}{2}} Y X^{-\frac{1}{2}})\|_F,$$

for $X, Y \in \mathcal{S}_{++}$ and $\sigma_1, \sigma_2 \in T_X \mathcal{S}_{++}$. Here $X^{\frac{1}{2}}$ denotes a square-root matrix satisfying $X = X^{\frac{1}{2}} X^{\frac{1}{2}}^T$. These definitions are independent of the choice of the square-root matrix (see Lemma B.1), and in practice the unique SPD square-root is used.

Given any function $f : \mathcal{S}_{++} \rightarrow \mathbb{R}$, its Riemannian gradient at X is

$$\text{grad}f(X) = X \nabla f(X) X \in T_X \mathcal{S}_{++},$$

where $\nabla f(X)$ is the Euclidean gradient. To move along a tangent vector $\sigma \in T_X \mathcal{S}_{++}$ for unit time along the geodesic, we use the exponential map:

$$\exp_X(\sigma) = X^{\frac{1}{2}} \exp(X^{-\frac{1}{2}} \sigma X^{-\frac{1}{2}}) X^{\frac{1}{2}},$$

with inverse given by the logarithmic map $\exp_X^{-1}(Y) = X^{\frac{1}{2}} \log(X^{-\frac{1}{2}} Y X^{-\frac{1}{2}}) X^{\frac{1}{2}}^T$. Gradient descent on f with step size Δt solves

$$X_{n+1} = \underset{X}{\operatorname{argmin}} \left\{ g_{X_n}(\exp_{X_n}^{-1}(X), \text{grad}f(X_n)) + \frac{1}{2\Delta t} d(X, X_n)^2 \right\},$$

this updates X analytically according to

$$(3.7) \quad X_{n+1} = X_n^{\frac{1}{2}} \exp\left(-\Delta t X_n^{\frac{1}{2}} \nabla f(X_n) X_n^{\frac{1}{2}}\right) X_n^{\frac{1}{2}}.$$

Take $f(C_k) = \text{KL}[\rho_a^{\text{GM}} \parallel \pi]$. Its gradient is given by $\nabla f(C_k) = \frac{w_k}{2} C_k^{-\frac{1}{2}} E_k(C_k) C_k^{-\frac{1}{2}}$. Then (3.7) is precisely the form used for the covariance update in (2.5). This also corresponds to mirror descent:

$$X_{n+1} = \underset{X}{\operatorname{argmin}} \left\{ \langle \nabla f(X_n), X - X_n \rangle + \frac{1}{\Delta t} D_\phi(X, X_n) \right\},$$

where $\langle \cdot, \cdot \rangle$ denotes the Frobenius inner product. The Bregman divergence is defined as $D_\phi(X, Y) = \phi(X) - \phi(Y) - \langle \nabla \phi(Y), X - Y \rangle$ with generator function $\phi(X) = \text{tr}(S_n \log S_n - S_n)$, where $S_n = X_n^{-\frac{1}{2}} X X_n^{-\frac{1}{2}}$. Note here ϕ is independent of the choice of square-root decomposition of X . The derivation uses the fact that $\nabla \phi(X) = X_n^{-1} \exp_{X_n}^{-1}(X) X_n^{-1}$.

Beyond the covariance update, the overall algorithm described in subsection 2.2 can be interpreted as a mirror descent scheme. This provides a new perspective for studying Gaussian mixture variational inference, including properties such as positivity preservation, affine invariance, and convergence. We formalize this connection in the following theorem, with the proof in section B.

THEOREM 3.5. *For the Gaussian mixture parameter vector*

$$a = [m_1, \dots, m_K, C_1, \dots, C_K, w_1, \dots, w_K],$$

we define the Bregman divergence $D_{\phi_n}(x, y) = \phi_n(x) - \phi_n(y) - \nabla \phi_n(y)^T (x - y)$ associated with the generator function

$$\phi_n(a) = \sum_{k=1}^K \left(\frac{w_{k,n}}{2} \text{tr}(S_{k,n} \log S_{k,n} - S_{k,n}) + \frac{w_{k,n}}{2} m_k^T C_{k,n}^{-1} m_k + w_k \log w_k \right),$$

where $S_{k,n} = C_{k,n}^{-\frac{1}{2}} C_k C_{k,n}^{-\frac{1}{2}}$. The proposed Gaussian mixture variational inference algorithm, with update rules (2.5)–(2.7), can be written in the form of mirror descent:

(3.8)

$$a_{n+1} = \underset{a}{\operatorname{argmin}} \left\{ \langle \nabla_a \text{KL}[\rho_a^{\text{GM}} \|\pi] |_{a_n}, a - a_n \rangle + \frac{1}{\Delta t_n} D_{\phi_n}(a, a_n) \right\} \quad \text{s.t.} \quad \sum_{k=1}^K w_k = 1.$$

Furthermore, consider an arbitrary invertible affine mapping $\psi : \theta \mapsto \tilde{\theta} = T\theta + d$. Let the transformed posterior distribution be $\tilde{\pi} = \psi \# \pi$, with potential $\tilde{\Phi}_R(\theta) = \Phi_R(T^{-1}(\theta - d))$. Then the algorithm remains invariant, with $\rho_{\tilde{a}}^{\text{GM}} = \psi \# \rho_a^{\text{GM}}$, namely the parameters and time step transform as follows:

$$\tilde{m}_k(t) = Tm_k(t) + d, \quad \tilde{C}_k(t) = TC_k(t)T^T, \quad \tilde{w}_k(t) = w_k(t), \quad \Delta \tilde{t}_n = \Delta t_n.$$

Remark 3.6. The potential function $\phi_n(a)$ in the mirror descent framework combines the covariance terms, the mean terms, and the weight terms, which induce the update of the three parts respectively. The resulting scheme is affine invariant at the discrete level, making the algorithm robust to coordinate transformations. In practice, as the result is independent of the decomposition method, Cholesky factorization is employed for efficient computation of matrix operations involving covariance matrices. \diamond

4. Implementation Details.

4.1. Scheduler. The scheduler $\eta(t)$ in (2.7) plays a crucial role in improving convergence, as demonstrated by both our theoretical analysis (See Theorem 3.4) and the experimental results that follow. We adopt the stable cosine decay—a variant of the scheduler proposed in [43, 40]—defined as

$$(4.1) \quad \eta(t_n) = \begin{cases} 1, & n \leq \frac{N}{2}, \\ \eta_{\min} + \frac{1-\eta_{\min}}{2} \left(1 + \cos \left(2\pi \left(\frac{n}{N} - \frac{1}{2} \right) \right) \right), & n > \frac{N}{2}, \end{cases}$$

where $\eta_{\min} < 1$, and N is the total number of iterations.

4.2. Annealing-based initialization. For multimodal posteriors or posteriors with heavy tails (See cases A and C in subsection 5.1), annealing can significantly improve exploration and approximation quality. Incorporating annealing into the variational framework is straightforward: the KL-divergence (1.2) is modified to:

$$\min_{\rho_a} \mathbb{E}_{\rho_a} [\log \rho_a] + \frac{1}{T} \mathbb{E}_{\rho_a} [\Phi_R],$$

where $T \geq 1$ controls the trade-off between the entropy and cross-entropy terms. Higher temperatures encourage exploration, helping Gaussian components move between modes instead of getting trapped in one.

In the present work, we employ an exponential annealing scheduler to reduce the temperature parameter T from an initial value T_{start} to 1 over N_α iterations, with $T_n = T_{\text{start}}^{\frac{N_\alpha - n}{N_\alpha - 1}}$ for $n = 1, \dots, N_\alpha$. The resulting distribution after the final iteration is used as the initial condition of GMBBVI. The initial value T_{start} is set such that the natural gradient of the entropy term dominates that of the cross-entropy term:

$$\left\| \frac{1}{T_{\text{start}}} \tilde{\nabla}_m \mathbb{E}_{\rho_a} [\Phi_R] \right\| \leq \alpha \cdot \|\tilde{\nabla}_m \mathbb{E}_{\rho_a} [\log \rho_a]\|,$$

where $\alpha \in (0, 1)$ is a small constant, and $\tilde{\nabla}_m$ denotes the natural gradient with respect to means m_1, \dots, m_K , using the same block-diagonal approximation of the Fisher information matrix as in subsection 2.1. This ensures early updates are entropy-driven for robust exploration. Here, we do not consider natural gradients based on the weights and covariance, as the primary goal during the annealing phase is to increase the separation between component means. These natural gradients are estimated in a derivative-free manner similar to (2.1).

5. Experimental results. In this section, we present numerical studies of the proposed GMBBVI method for sampling complex distributions of unknown parameters or fields¹. Specifically, we consider the following examples:

1. Multi-dimensional model problems (up to 50 dimensions): We use these problems to demonstrate that GMBBVI is robust with respect to distributions featuring multiple modes, infinitely many modes, and modes with narrow and curved shapes. Additionally, we benchmark BBVI against Neal's funnel using WALNUTS [45], the state-of-the-art derivative-based sampling approach for this case, to highlight the strengths and limitations of our method.
2. Darcy flow problem: We consider the inverse problem of recovering the permeability field of a Darcy flow equation. The problem is structured to exhibit symmetry, resulting in two modes in the posterior. We demonstrate that GMBBVI effectively captures both modes, illustrating its potential for tackling multimodal problems in large-scale, moderate-dimensional applications.

For all experiments, we set $\Delta t_{\text{max}} = \beta = 0.9$ in (2.7), adopt the stable cosine decay scheduler mentioned in (4.1) decreasing from 1 to 0.1, and use $J = 4N_\theta$ samples for each Gaussian integral in (2.3).

5.1. Multi-dimensional model problems. In this subsection, we first investigate several classical 2D sampling problems, together with their modified higher-dimensional counterparts in 10 and 50 dimensions. For the 2D setting, we consider the following problems:

¹Our code is available online for reproducibility: <https://github.com/PKU-CMEGroup/InverseProblems.jl/tree/master/Derivative-Free-Variational-Inference>.

Case A : The target distribution is a Gaussian mixture with 10 modes that are well separated (See [Figure 1](#)).

Case B : The target distribution has a circular geometry [[17](#), Appendix E] and contains infinitely many modes. It is defined by

$$\Phi_R(\theta) = \frac{1}{2} \mathcal{F}(\theta)^T \mathcal{F}(\theta), \text{ where } \mathcal{F}(\theta) = \frac{y - (\theta_{(1)}^2 + \theta_{(2)}^2)}{0.3} \text{ and } y = 1.$$

Case C : The target distribution is based on the Rosenbrock function, which exhibits the characteristic “banana-shaped” geometry [[25](#)]. It is given by

$$\Phi_R(\theta) = \frac{1}{2} \mathcal{F}(\theta)^T \mathcal{F}(\theta), \text{ where } \mathcal{F}(\theta) = \frac{1}{\sqrt{10}} \begin{pmatrix} y - \left[\begin{matrix} 10(\theta_{(2)} - \theta_{(1)}^2) \\ \theta_{(1)} \end{matrix} \right] \end{pmatrix}, y = \begin{bmatrix} 0 \\ 1 \end{bmatrix}.$$

We then modify these sampling problems to an N_θ -dimensional setting ($N_\theta = 10, 50$) by introducing $N_\theta - 2$ additional variables θ^c . For Case A, the latter $N_\theta - 2$ dimensions are modeled as independent Gaussian random variables, each with a mean of $m_i \sim \mathcal{N}(0, 1)$ and a variance of 1. For Cases B and C, the reference density is defined with

$$\Phi_R(\theta, \theta^c) = \frac{1}{2} \mathcal{F}(\theta)^T \mathcal{F}(\theta) + \frac{1}{2} (\theta^c - K\theta)^T (\theta^c - K\theta),$$

where $\theta \in \mathbb{R}^2, \theta^c \in \mathbb{R}^{N_\theta-2}$, and $K \in \mathbb{R}^{(N_\theta-2) \times 2}$ is an all-ones matrix. These high-dimensional target densities are constructed so that the marginal densities of θ are analytically tractable and coincide exactly with the corresponding 2D target density.

We apply GMBBVI with $K = 40$ modes, initialized with means $m_i \sim \mathcal{N}(0, I)$ and covariances $C_i = I$, and run the algorithm for 500 iterations. For Cases A and C, the annealing strategy described in [subsection 4.2](#) with $N_\alpha = 500$ and $\alpha = 0.1$ is employed to address multimodality and heavy-tailed behavior. The resulting marginal densities and convergence in terms of total variation(TV) distance are shown in [Figure 1](#), with each row corresponding to one case (Cases A-C). For the cases considered, GMBBVI effectively captures multiple modes and provides a good approximation to the target distribution, converging within $\mathcal{O}(10^2)$ iterations to achieve a TV distance below 0.1 for moderately high-dimensional problems.

Next, we consider a challenging benchmark known as Neal’s funnel [[46](#)], defined as

$$\theta_{(1)} \sim \mathcal{N}(0, 9), \quad \theta_{(i)} \mid \theta_{(1)} \sim \mathcal{N}(0, e^{\theta_{(1)}}), \quad i = 2, \dots, N_\theta.$$

The joint distribution exhibits a funnel-like geometry, with $\theta_{(1)}$ forming the funnel axis. This distribution can be viewed as a model problem for Bayesian hierarchical models. The multiscale behavior of the funnel makes it particularly challenging; we expect our GMBBVI to adapt to the local geometry by using different Gaussian components. We also employ the recently proposed WALNUTS [[45](#)], which is an improved variant of the No-U-Turn sampler [[31](#)] for this benchmark.

We apply GMBBVI with $K = 40$ modes, initialized with means $m_i \sim \mathcal{N}(0, I)$ and covariances $C_i = I$, and run the algorithm for 2000 iterations. For WALNUTS, we adopt the parameter settings from [[45](#)], utilizing WALNUTS-R2P and 1000 warm-up iterations with $H = 0.3$ and $\delta = 0.3$ for a total 16000 accepted proposals. Comparative results, including marginal densities and several convergence metrics, are presented in [Figure 2](#), where each row corresponds to a dimensional setting ($N_\theta = 2, 10, 50$). The results indicate that GMBBVI achieves accuracy comparable to WALNUTS in low-dimensional settings ($N_\theta = 2, 10$), while offering a clear computational speed

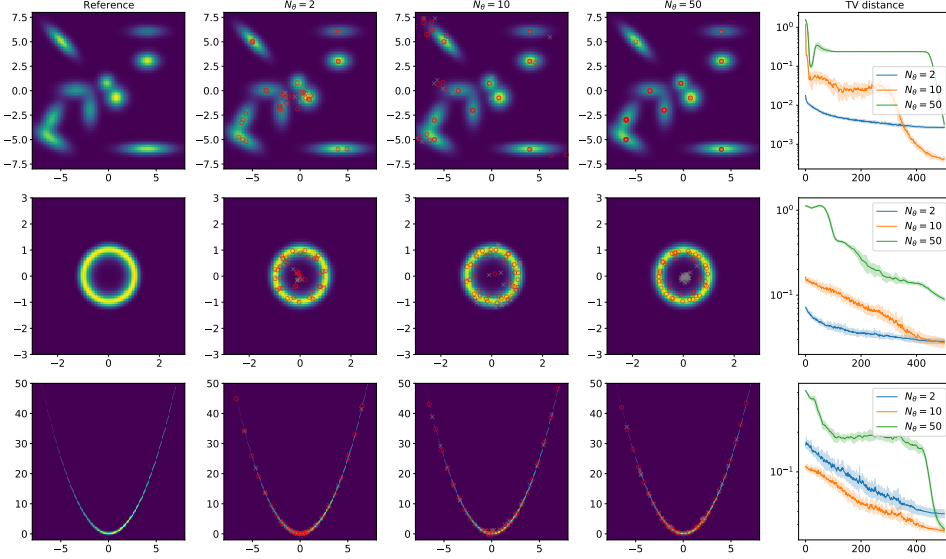


Fig. 1: Multi-dimensional model problems: Cases A to C are arranged from the top row to the bottom row. Each panel shows the reference marginal density along with the GMBBVI estimates for problem dimensions 2, 10, 50 (from left to right). The projected means of each Gaussian component are marked by red circles, and the projected means at iteration 0 (after annealing) are marked by grey crosses. The fifth panel displays the total variation distance between the reference marginal density and the estimated marginal densities across the iterations, with shaded area representing the standard deviation computed from 10 independent trials.

advantage. However, in higher dimensions ($N_\theta = 50$), GMBBVI fails to provide reliable marginal variance estimates compared with WALNUTS. This limitation arises because Gaussian components become trapped and oscillate in transverse directions near the narrow neck of the funnel, making exploration along the axial direction inefficient.

Finally, we demonstrate that GMBBVI is robust with respect to the initial condition, the scheduler η , the annealing parameter, and a sufficiently large number of modes K . Detailed sensitivity results are presented in [Section C](#).

5.2. Darcy flow problem. In this subsection, we evaluate our proposed GMBBVI algorithm on a Bayesian inverse problem arising from the Darcy flow equation on the two-dimensional spatial domain $D = [0, 1]^2$. This equation characterizes the pressure field $p(x)$ in a porous medium governed by a positive permeability field $a(x, \theta)$:

$$(5.1) \quad -\nabla \cdot (a(x, \theta) \nabla p(x)) = f(x), \quad x \in D,$$

subject to homogeneous Dirichlet boundary conditions $p(x) = 0$ on ∂D for simplicity. The fluid source field f is defined piecewise in the x_2 direction as follows: it takes value 1000 for $x_2 \leq \frac{4}{6}$, 2000 for $\frac{4}{6} < x_2 \leq \frac{5}{6}$, and 3000 for $\frac{5}{6} < x_2 \leq 1$. The logarithm of the permeability field $\log a(x_1, x_2)$ is parameterized via a Karhunen-Loëve (KL)

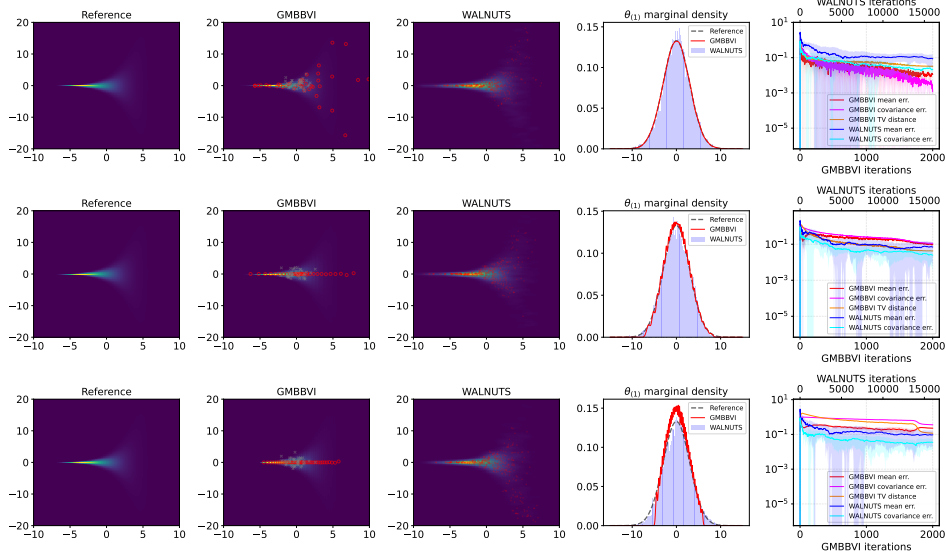


Fig. 2: Neal’s funnel model problem: Dimensions 2, 10, and 50 are arranged from the top row to the bottom row. Each panel shows the reference marginal density of $(\theta_{(1)}, \theta_{(2)})$ along with the GMBBVI and WALNUTS estimates (from left to right). For GMBBVI, the projected means of each Gaussian component are marked by red circles, and the initializations are marked by grey crosses. For WALNUTS, red dots denote the last 5000 particles, and the marginal density is visualized using kernel density estimation. The fourth panel displays the reference marginal density of $\theta_{(1)}$ along with the GMBBVI and WALNUTS estimates. The fifth panel reports convergence metrics for $\theta_{(1)}$, including its mean and variance, for both methods, as well as the total variation distance between the reference marginal density and the GMBBVI estimates of $(\theta_{(1)}, \theta_{(2)})$, with the shaded area representing the standard deviation computed from 10 independent trials.

expansion:

$$(5.2) \quad \log a(x_1, x_2) = \sum_l \theta_l \sqrt{\lambda_l} \phi_l(x_1, x_2).$$

Here the summation is taken over $l = (l_1, l_2) \in \mathbb{Z}^{0+} \times \mathbb{Z}^{0+} \setminus \{(0, 0)\}$, $\{\lambda_l\}$ denotes the eigenvalues arranged in descending order as

$$(5.3) \quad \lambda_l = (\pi^2(l_1^2 + l_2^2) + \tau^2)^{-d},$$

where $d = 2.0$ and $\tau = 3.0$ are parameters governing the decay rate of the eigenvalues. The corresponding eigenfunctions $\{\phi_l\}$ are defined as:

$$(5.4) \quad \phi_l(x_1, x_2) = \begin{cases} \sqrt{2} \cos(\pi l_1 x_1), & \text{if } l_2 = 0, \\ \sqrt{2} \cos(\pi l_2 x_2), & \text{if } l_1 = 0, \\ 2 \cos(\pi l_1 x_1) \cos(\pi l_2 x_2), & \text{otherwise.} \end{cases}$$

For numerical implementation, we truncate the KL expansion (5.2) to its first $N_\theta = 32$ terms and solve the Darcy flow equation (5.1) using the finite difference

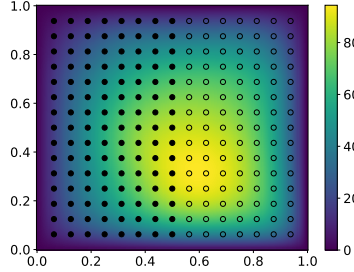


Fig. 3: Darcy flow problem: The pressure field and symmetry observations at 120 equidistant points (solid black dots). Their mirroring points are marked (empty black dots).

method, where the computational domain is discretized by a 80×80 uniform grid. The observations y_{obs} in the inverse problem are selected as the symmetric pressure sum $\frac{1}{2}[p(x_1, x_2) + p(1 - x_1, x_2)]$ evaluated at 120 equidistant points in the left region of the domain (see Figure 3), thereby inducing the forward mapping $\mathcal{G} : \theta \in \mathbb{R}^{32} \mapsto y \in \mathbb{R}^{120}$. The Bayesian inverse problem aims to sample from the posterior distribution of θ , given by

$$\rho_{\text{post}}(\theta) \propto \exp \left(-\frac{1}{2\sigma_\eta^2} \|y_{\text{obs}} - \mathcal{G}(\theta)\|^2 - \frac{1}{2\sigma_0^2} \|\theta\|^2 \right).$$

Here we adopt the prior distribution of θ as $\mathcal{N}(0, \sigma_0^2 I_{32})$, and y_{obs} represents the observation corrupted by noise $\eta \sim \mathcal{N}(0, \sigma_\eta^2 I_{120})$, with $\sigma_0 = 5.0$ and $\sigma_\eta = 0.25$. Due to the symmetric nature of our observations and fluid source field, symmetric permeability fields induce identical observations, rendering the aforementioned posterior distribution at least bimodal.

In our inverse problem setup, we randomly select θ_{ref} according to the prior distribution, obtain the corresponding permeability field, and solve the Darcy flow equation (5.1) on a grid refined by a factor of three. Additive noise following $\mathcal{N}(0, \sigma_\eta^2 I_{120})$ is incorporated into the observation y_{obs} .

We run GMBBVI for 500 iterations, with $K = 5$ modes where each mean is initialized according to $\mathcal{N}(0, \sigma_0^2 I)$ and each covariance is set to $\sigma_0^2 I$. Upon completion of the iterations, we compare the logarithm of permeability fields corresponding to each m_k against the true and mirror permeability fields to partition them into two groups. The weighted means of m_k within each group are computed to reconstruct the permeability fields, as presented in Figure 4. The evolution curves of various metrics during iterations are shown in Figure 5, illustrating that GMBBVI converges in around 100 iterations. Additionally, Figure 6 displays the marginal distributions of the Gaussian mixture on the first 16 dimensions. These results demonstrate that our algorithm GMBBVI achieves rapid convergence without requiring derivatives of \mathcal{G} , while successfully capturing the multimodal nature of the posterior distribution.

6. Conclusions. In this paper, we investigate stability issues in Gaussian mixture black-box variational inference methods. We propose an adaptive exponential time integrator and demonstrate its superior stability and efficiency in approximating moderately high-dimensional probability distributions through both theoretical analysis and empirical validation.

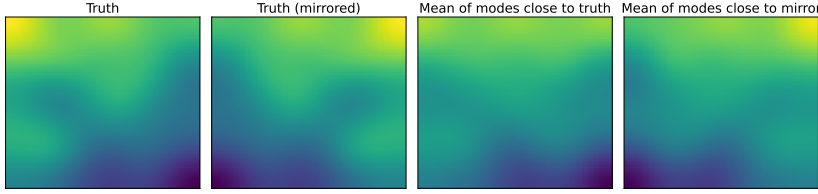


Fig. 4: Darcy flow problem: The true initial permeability field (leftmost), its mirrored field (middle-left), recovered permeability fields by modes close to truth (middle-right) and close to mirrored truth (rightmost).

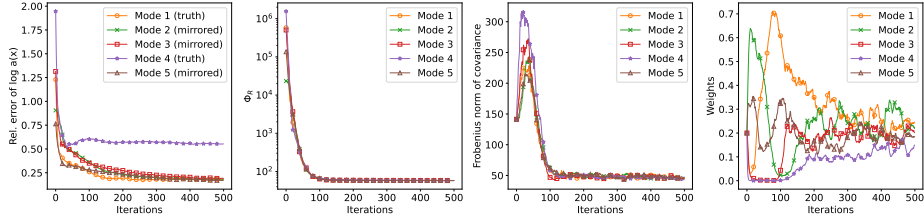


Fig. 5: The relative errors of the logarithm of permeability field, the optimization errors $\Phi_R(m_k)$, the Frobenius norm $\|C_k\|_F$, and the Gaussian mixture weights w_k (from left to right) for different modes over GMBVI iterations.

Several promising directions for future research remain. On the algorithmic side, the proposed exponential integrator and its connections to manifold optimization and mirror descent could also be extended to other gradient-based sampling methods involving covariance matrices or other constrained manifolds. On the theoretical side, a more detailed analysis of the approximation capabilities and optimization guarantees of Gaussian mixtures and related variational approaches for general target distributions beyond Gaussians, including log-concave densities, would provide deeper insights into their practical performance and limitations.

Acknowledgments. We acknowledge the support of the high-performance computing platform of Peking University.

Appendix A. Proof for the Convergence.

Derivation of (3.2) and (3.3). For the Gaussian case that $\Phi_R(\theta) = \frac{1}{2}(\theta - m_\star)^T C_\star^{-1}(\theta - m_\star)$, and following the definitions in (2.2) and (3.1), we have

$$(A.1) \quad \begin{aligned} f(t_n, \theta) &= -\frac{1}{2}\theta^T \theta + \frac{1}{2}(L(t_n)\theta + m(t_n) - m_\star)^T C_\star^{-1}(L(t_n)\theta + m(t_n) - m_\star) + \text{const} \\ &= \frac{1}{2}\theta^T (L_n^T L_n - I)\theta + v_n^T L_n \theta + \frac{1}{2}\|v_n\|^2 + \text{const},. \end{aligned}$$

Then we have

$$\begin{aligned} \mathbb{E}_\mathcal{N} \left[\theta(f - \mathbb{E}_\mathcal{N}[f]) \right] &= \mathbb{E}_\mathcal{N}[\nabla_\theta f] = L_n^T v_n, \\ \mathbb{E}_\mathcal{N} \left[\theta \theta^T (f - \mathbb{E}_\mathcal{N}[f]) \right] &= \mathbb{E}_\mathcal{N}[\nabla_\theta \nabla_\theta f] = L_n^T L_n - I. \end{aligned}$$

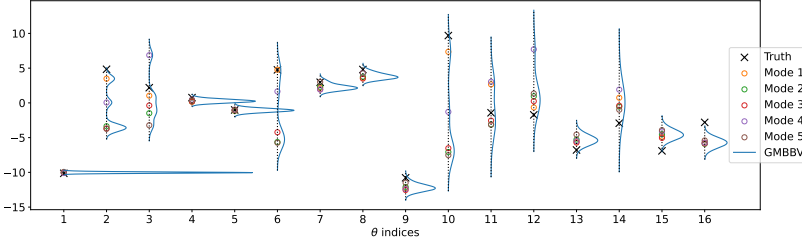


Fig. 6: The true KL expansion parameters $\theta_{(i)}$ (black crosses), and mean estimations of $\theta_{(i)}$ for each mode (circles) and the associated marginal distributions obtained by GMBBVI at the 500th iteration, only the first 16 dimensions are plotted.

Using these calculations and the update schemes in (2.5) and (2.6), we obtain

$$\begin{aligned} v_{n+1} &= v_n - \Delta t_n \mathbf{L}_n \mathbf{L}_n^T v_n = (I - \Delta t_n \Sigma_n) v_n \\ \Sigma_{n+1} &= \mathbf{L}_n e^{-\Delta t_n (\mathbf{L}_n^T \mathbf{L}_n - I)} \mathbf{L}_n^T = \Sigma_n \mathbf{L}_n^{-T} e^{\Delta t_n (I - \mathbf{L}_n^T \mathbf{L}_n)} \mathbf{L}_n^T \\ &= \Sigma_n e^{\Delta t_n \mathbf{L}_n^{-T} (I - \mathbf{L}_n^T \mathbf{L}_n) \mathbf{L}_n^T} = \Sigma_n e^{\Delta t_n (I - \Sigma_n)} = h_n(\Sigma_n), \end{aligned}$$

where h_n is defined in (3.3). That finishes the derivation of (3.2) and (3.3).

Proof of Theorem 3.1. We first consider the convergence of $\{\Sigma_n\}$. Let $x_n^i (1 \leq i \leq N_\theta)$ denote the eigenvalues of Σ_n , ordered increasingly. Writing the eigen decomposition as $\Sigma_n = P^T \Lambda_n P$, the update rule gives

$$\Sigma_{n+1} = P^T h_n(\Lambda_n) P, \quad \text{with } \Lambda_{n+1} = h_n(\Lambda_n) \text{ diagonal.}$$

Therefore, these eigenvalues evolve according to the iteration $h_n(x)$, and are reordered after each step.

We outline several properties of $h_n(x) = x e^{\Delta t_n (1-x)}$ for scalar $x > 0$ with $0 < \Delta t_n \leq 1$. First, its derivative is $h'_n(x) = e^{\Delta t_n (1-x)} (1 - \Delta t_n x)$, so $h_n(x)$ is increasing up to its maximum at $x = \frac{1}{\Delta t_n} \geq 1$, and decreasing thereafter, hence

$$(A.2) \quad h_n(x) \leq h_n\left(\frac{1}{\Delta t_n}\right).$$

Second, for $x < 1$, $h_n(x) > x$ since $e^{\Delta t_n (1-x)} > 1$, and $h_n(x) < 1$, since $h_n(x) < h_n(1) = 1$. For $x > 1$, $h_n(x) < x$ since $e^{\Delta t_n (1-x)} < 1$, and moreover, $|h_n(x) - 1| < x - 1$. If $h_n(x) > 1$, this is immediate; if $h_n(x) < 1$, the inequality follows the fact $2 < x(1 + e^{1-x}) \leq x(1 + e^{\Delta t_n (1-x)})$ with $x > 1$. Therefore, for $x > 0$, we have

$$(A.3) \quad |h_n(x) - 1| \leq |x - 1|,$$

with equality only at $x = 1$. This property implies that all eigenvalues move closer to 1 at each iteration, including the largest and smallest eigenvalues.

Step 1. Warm-up phase for large eigenvalues. We first show that after a warm-up phase of $N_1 = \mathcal{O}(|\ln \lambda_{\max}(\Sigma_0)|)$ iterations, the adaptive time step remains uniformly bounded away from 0, independent of initialization. By definition,

$$\Delta t_n = \min\left\{\frac{\beta}{\|\Sigma_n - I\|_2}, \Delta t_{\max}\right\} = \min\left\{\frac{\beta}{|x_n^{N_\theta} - 1|}, \frac{\beta}{|1 - x_n^1|}, \Delta t_{\max}\right\}.$$

Suppose $x_n^{N_\theta} > 1$; otherwise, $\Delta t_n \geq \min\{\beta, \Delta t_{\max}\}$. We show that the largest eigenvalue, $x_{n+1}^{N_\theta} = \max_{1 \leq i \leq N_\theta} \{h_n(x_n^i)\}$, decreases exponentially until it enters a bounded domain. Indeed,

$$(A.4) \quad x_{n+1}^{N_\theta} \leq \max\left\{\frac{1}{\Delta t_{\max}} e^{\Delta t_{\max}-1}, \frac{2}{\beta} e^{\frac{\beta}{2}-1}, x_n^{N_\theta} e^{-\beta}, x_n^{N_\theta} e^{\frac{\beta}{2}-1}\right\}.$$

This bound reflects three possible cases:

1. If $\Delta t_n = \Delta t_{\max}$, then $h_n(x) \leq h_n(\frac{1}{\Delta t_n}) = \frac{1}{\Delta t_{\max}} e^{\Delta t_{\max}-1}$.
2. If $\Delta t_{\max} > \Delta t_n$ and $\Delta t_n > \frac{\beta}{2}$, then $h_n(x) \leq h_n(\frac{1}{\Delta t_n}) \leq \frac{2}{\beta} e^{\frac{\beta}{2}-1}$.
3. If $\Delta t_{\max} > \Delta t_n$ and $\Delta t_n < \frac{\beta}{2}$, then $\Delta t_n = \frac{\beta}{x_n^{N_\theta}-1}$ and $h_n(x_n^i) = x_n^i e^{-\beta \frac{x_n^i-1}{x_n^{N_\theta}-1}}$. The maximum occurs either at $x_n^{N_\theta}$ or at $\frac{x_n^{N_\theta}-1}{\beta}$. For the first case, $h_n(x_n^{N_\theta}) = x_n^{N_\theta} e^{-\beta}$; For the second case, requiring $\frac{x_n^{N_\theta}-1}{\beta} \leq x_n^{N_\theta}$, we have $h_n(\frac{x_n^{N_\theta}-1}{\beta}) = \frac{x_n^{N_\theta}-1}{\beta} e^{\frac{\beta}{x_n^{N_\theta}-1}-1} \leq x_n^{N_\theta} e^{\frac{\beta}{2}-1}$.

Therefore after

$$(A.5) \quad N_1 = \frac{\ln \lambda_{\max}(\Sigma_0)}{\min\{\beta, 1 - \frac{\beta}{2}\}} = \mathcal{O}(|\ln \lambda_{\max}(\Sigma_0)|)$$

iterations, we obtain for all $n \geq N_1$:

$$(A.6) \quad x_n^{N_\theta} \leq x_{\max}^{N_\theta} := \max\left\{\frac{1}{\Delta t_{\max}} e^{\Delta t_{\max}-1}, \frac{2}{\beta} e^{\frac{\beta}{2}-1}\right\},$$

and consequently,

$$(A.7) \quad \Delta t_n \geq \Delta t_{\min} := \min\left\{\frac{\beta}{x_{\max}^{N_\theta}-1}, \beta, \Delta t_{\max}\right\}.$$

Step 2. Convergence phase for large eigenvalues. We then prove that after a convergence phase with $N_2 = \mathcal{O}(\ln \frac{1}{\epsilon})$ iterations, the largest eigenvalue satisfies $x_n^{N_\theta} \leq 1 + \epsilon$. From (A.3), $h_n(x)$ for $x > 1$ is a contraction:

$$h_n(x) - h_n(1) = h_n'(\xi)(x-1) = e^{\Delta t_n(1-\xi)}(1 - \Delta t_n \xi)(x-1) \quad \text{with } 1 < \xi < x.$$

Either $h_n(x)$ falls below 1, or the contraction factor satisfies $e^{\Delta t_n(1-\xi)}(1 - \Delta t_n \xi) \leq 1 - \Delta t_{\min}$, since $\Delta t_n \geq \Delta t_{\min}$ from (A.7) and $\xi > 1$. Then, after

$$(A.8) \quad N_2 = \frac{\ln \frac{1}{\epsilon} + \ln(x_{\max}^{N_\theta} - 1)}{\ln \frac{1}{1 - \Delta t_{\min}}} = \mathcal{O}(\ln \frac{1}{\epsilon})$$

iterations, we obtain $x_n^{N_\theta} \leq \epsilon + 1$. By (A.3), during subsequent iterations, these eigenvalues greater than 1 then remain in $(1 - \epsilon, 1 + \epsilon)$ and continue to converge toward 1.

Step 3. Warm-up phase for small eigenvalues. Next, we consider the smallest eigenvalue, $x_{n+1}^1 = \min_{1 \leq i \leq N_\theta} \{h_n(x_n^i)\}$. We will show that after an additional warm-up phase of $N_3 = \mathcal{O}(|\ln \lambda_{\min}(\Sigma_0)|)$ iterations, all eigenvalues becomes greater than $1 - \delta$ with $\delta = \frac{1}{3}$. After the previous phases ($N_1 + N_2$ iterations), we have

$$\lambda_{\min}(\Sigma_n) \geq \min\{\lambda_{\min}(\Sigma_0), e^{-\beta}\},$$

since eigenvalues with $x_n^i < 1$ continue to increase, while those with $x_n^i > 1$ remain bounded below by $h_n(x_n^i) = x_n^i e^{\Delta t_n(1-x_n^i)} \geq x_n^i e^{-\beta} > e^{-\beta}$. When the smallest eigenvalue satisfies $x_n^1 < 1 - \delta$, we have

$$-\ln x_{n+1}^1 = \max_i \{-\ln x_n^i - \Delta t_n(1 - x_n^i)\} \leq -\ln x_n^1 - \Delta t_{\min} \delta.$$

Then after

$$(A.9) \quad N_3 = \frac{\max\{-\ln \lambda_{\min}(\Sigma_0), \beta\}}{\Delta t_{\min} \delta} = \mathcal{O}(|\ln \lambda_{\min}(\Sigma_0)|)$$

iterations, the smallest eigenvalue becomes larger than $1 - \delta$.

Step 4. Convergence phase for small eigenvalues. Finally, we consider the convergence phase for the smallest eigenvalue. After $N_4 = \mathcal{O}(\ln \frac{1}{\epsilon})$ iterations, it satisfies $x_n^1 \geq 1 - \epsilon$. Again, $h_n(x)$ for $1 - \delta < x < 1$ is a contraction:

$$h_n(1) - h_n(x) = h_n'(\xi)(1 - x) = e^{\Delta t_n(1-\xi)}(1 - \Delta t_n \xi)(1 - x) \quad \text{with } x < \xi < 1.$$

Using $\delta = \frac{1}{3}$, the contraction rate can be bounded as

$$\begin{aligned} e^{\Delta t_n(1-\xi)}(1 - \Delta t_n \xi) &\leq e^{\Delta t_n \delta}(1 - \Delta t_n(1 - \delta)) \\ &\leq \frac{1}{1 - \Delta t_n \delta}(1 - \Delta t_n(1 - \delta)) \leq 1 - \delta \Delta t_n \leq 1 - \delta \Delta t_{\min}. \end{aligned}$$

Here, the first inequality uses the fact that the expression is decreasing with respect to ξ ; in the second inequality we use $e^a \leq \frac{1}{1-a}$ for $a \in (0, 1)$; the third inequality uses that $\delta = \frac{1}{3}$; and the last inequality uses the lower bound $\Delta t_n \geq \Delta t_{\min}$. Therefore, after

$$(A.10) \quad N_4 = \frac{\ln \frac{1}{\epsilon}}{\ln \frac{1}{1 - \delta \Delta t_{\min}}} = \mathcal{O}(\ln \frac{1}{\epsilon})$$

iterations, we have $x_n^1 \geq 1 - \epsilon$.

Then we consider the convergence of $\{v_n\}$. Since $\|v_{n+1}\|_2 = \|I - \Delta t_n \Sigma_n\|_2 \|v_n\|_2$, it suffices to bound the spectral norm of $I - \Delta t_n \Sigma_n$. Using the upper bound on Δt_n in (3.4) and the assumptions $\Delta t_{\max}, \beta \leq 1$, we obtain

$$I \succeq I - \Delta t_n \Sigma_n = (1 - \Delta t_n)I + \Delta t_n(I - \Sigma_n) \succeq (1 - \Delta t_{\max} - \beta)I \succeq -I.$$

Consequently, $\|v_n\|_2$ is non-increasing. If $\|v_0\|_2 \leq \epsilon$, the sequence has already converged. Otherwise, after the four steps described above, we have the refined bounds hold: $(1 - (1 + \epsilon)\Delta t_{\max}) \preceq I - \Delta t_n \Sigma_n \preceq (1 - (1 - \epsilon)\Delta t_{\min})I$, where $\epsilon < 1$, $\Delta t_{\max} < 1$, and $\Delta t_{\min} > 0$ is defined in (A.7). Therefore after

$$(A.11) \quad N_5 = \frac{\ln \frac{1}{\epsilon} + \max\{\ln \|v_0\|_2, 0\}}{\ln \frac{1}{\max\{(1+\epsilon)\Delta t_{\max}-1, 1-(1-\epsilon)\Delta t_{\min}\}}} = \mathcal{O}\left(\ln \frac{1}{\epsilon} + \max\{\ln \|v_0\|_2, 0\}\right) \quad \square$$

iterations, we have $\|v_n\|_2 \leq \epsilon$.

Combining all phases, after $N_1 + N_2 + N_3 + N_4 + N_5$ iterations as defined in (A.5) and (A.8)–(A.11), all eigenvalues of Σ_n lie in the interval $(1 - \epsilon, 1 + \epsilon)$, and the norm of v_n is below ϵ , which completes the proof of (3.5).

Proof of Theorem 3.4. **Step 1. Derivation of the tail bounds of error terms.** Recall from (A.1) that $f(t_n, \theta) = \frac{1}{2}\theta^T(\mathbf{L}_n^T \mathbf{L}_n - I)\theta + v_n^T \mathbf{L}_n \theta + \text{const}$, which is a quadratic function of θ . Under Assumption 1, the coefficients are uniformly bounded. We employ Monte Carlo sampling with $\theta \sim \mathcal{N}(0, I)$ to estimate $\mathbb{E}_{\mathcal{N}}[\theta \theta^T(f - \mathbb{E}_{\mathcal{N}}[f])]$ and $\mathbb{E}_{\mathcal{N}}[\theta(f - \mathbb{E}_{\mathcal{N}}[f])]$. The corresponding Monte Carlo error terms are bounded by polynomial functions of $\|\theta\|_2$. Since the Gaussian tail bound $\mathbb{P}_{\theta \sim \mathcal{N}}[\|\theta\|_2^p \geq t] \lesssim e^{-t^{\frac{2}{p}}}$, it follows that there exist constants $C_1, C_2, \gamma > 0$ such that

$$(A.12) \quad \mathbb{P}(\|\Omega_n\|_2 > t | \mathcal{F}_n) < C_1 e^{-C_2 t^\gamma}, \quad \mathbb{P}(\|\tilde{w}_n\|_2 > t | \mathcal{F}_n) < C_1 e^{-C_2 t^\gamma},$$

where \mathcal{F}_n is a filtration defined by $\mathcal{F}_n = \sigma(\{\Sigma_k, v_k\}_{1 \leq k \leq n})$.

Step 2. Probability Estimate for the Adaptive Time-Step Selection. Recall that the time step is $\Delta t_n = \min\{\eta(t_n)\Delta t_{\max}, \frac{\beta}{\|-\mathbf{L}_n^T \mathbf{L}_n + I + \Omega_n\|_2}\}$. Define

$$k_n = \frac{\beta}{\Delta t_{\max} \eta(t_n)}, \quad A_n = \{\Delta t_n = \frac{\beta}{\|-\mathbf{L}_n^T \mathbf{L}_n + I + \Omega_n\|_2}\} = \{\|-\mathbf{L}_n^T \mathbf{L}_n + I + \Omega_n\|_2 \geq k_n\}. \blacksquare$$

Then

$$\begin{aligned} \mathbb{P}(A_n | \mathcal{F}_n) &\leq \mathbb{P}(\|\Omega_n\|_2 \geq k_n - \|\mathbf{L}_n^T \mathbf{L}_n - I\|_2 | \mathcal{F}_n) \\ &\leq \mathbb{P}(\|\mathbf{L}_n^T \mathbf{L}_n - I\|_2 > \frac{k_n}{2} | \mathcal{F}_n) + \mathbb{E}(1_{\{\|\mathbf{L}_n^T \mathbf{L}_n - I\|_2 \leq \frac{k_n}{2}\}} 1_{\{\|\Omega_n\|_2 \geq k_n - \|\mathbf{L}_n^T \mathbf{L}_n - I\|_2\}} | \mathcal{F}_n) \\ &\leq \frac{\|\Sigma_n - I\|_2^2}{(k_n/2)^2} + C_1 e^{-\frac{C_2}{2^\gamma} k_n^\gamma}, \end{aligned} \blacksquare$$

where the last inequality follows from Markov's inequality and the tail bound in (A.12). By Assumption 1, there exists $C_0 > 0$ such that $\mathbb{E}[\|\Sigma_n\|_2^2] < C_0^2$. Moreover, using the inequality $e^{-\frac{1}{x}} \lesssim x^{\frac{2}{\gamma}}$ when $x > 0$ to bound the exponential term, we obtain

$$\begin{aligned} \mathbb{P}(A_n | \mathcal{F}_n) &\leq \frac{2\|\Sigma_n\|_2^2 + 2}{(k_n/2)^2} + C_1 e^{-\frac{C_2 \beta^\gamma}{2^\gamma \Delta t_{\max} \eta(t_n)^\gamma}} \\ (A.13) \quad &\leq \frac{8(C+1)\Delta t_{\max}^2}{\beta^2} \eta(t_n)^2 + C_3 \eta(t_n)^2 = \left(\frac{8(C+1)\Delta t_{\max}^2}{\beta^2} + C_3\right) \eta(t_n)^2, \end{aligned}$$

for some constant $C_3 > 0$. Since $\sum_{n=1}^{\infty} \eta(t_n)^2 < \infty$, it follows that $\sum_{n=1}^{\infty} \mathbb{P}(A_n) < \infty$. By Borel-Cantelli Lemma, we have $\mathbb{P}(A_n, i.o.) = 0$.

Step 3. Σ_n converges to I almost surely. Define the Lyapunov function $V(\Sigma) = \text{tr}(\Sigma - \log \Sigma - I)$. From the update rule, we obtain

$$\begin{aligned} V(\Sigma_{n+1}) - V(\Sigma_n) &= \text{tr}(\mathbf{L}_n(e^{\Delta t_n(-\mathbf{L}_n^T \mathbf{L}_n + I + \Omega_n)} - I)\mathbf{L}_n^T) \\ (A.14) \quad &\quad - \left(\text{tr}(\log(\mathbf{L}_n e^{\Delta t_n(-\mathbf{L}_n^T \mathbf{L}_n + I + \Omega_n)} \mathbf{L}_n^T)) - \text{tr}(\log \Sigma_n) \right). \end{aligned}$$

Since $e^x - 1 \leq x + x^2$ for $|x| \leq 1$ and $\|\Delta t_n(-\mathbf{L}_n^T \mathbf{L}_n + I + \Omega_n)\|_2 \leq \beta \leq 1$, we obtain

$$\begin{aligned} \text{tr}(\mathbf{L}_n(e^{\Delta t_n(-\mathbf{L}_n^T \mathbf{L}_n + I + \Omega_n)} - I)\mathbf{L}_n^T) &\leq \text{tr}\left(\mathbf{L}_n(\Delta t_n(-\mathbf{L}_n^T \mathbf{L}_n + I + \Omega_n) + (\Delta t_n)^2(-\mathbf{L}_n^T \mathbf{L}_n + I + \Omega_n)^2)\mathbf{L}_n^T\right) \\ (A.15) \quad &= \Delta t_n \text{tr}(\mathbf{L}_n^T \mathbf{L}_n(-\mathbf{L}_n^T \mathbf{L}_n + I + \Omega_n)) + (\Delta t_n)^2 \text{tr}(\mathbf{L}_n^T \mathbf{L}_n(-\mathbf{L}_n^T \mathbf{L}_n + I + \Omega_n)^2). \blacksquare \end{aligned}$$

Note that $\log \det \Sigma = \text{tr} \log \Sigma$, we further obtain

$$\begin{aligned} \text{tr}(\log(\mathbf{L}_n e^{\Delta t_n(-\mathbf{L}_n^T \mathbf{L}_n + I + \Omega_n)} \mathbf{L}_n^T)) - \text{tr}(\log \Sigma_n) &= \log \det(\mathbf{L}_n e^{\Delta t_n(-\mathbf{L}_n^T \mathbf{L}_n + I + \Omega_n)} \mathbf{L}_n^T) - \log \det \Sigma_n \\ (A.16) \quad &= \Delta t_n \text{tr}(-\mathbf{L}_n^T \mathbf{L}_n + I + \Omega_n). \blacksquare \end{aligned}$$

Substituting (A.15) and (A.16) into (A.14) and taking conditional expectations with respect to \mathcal{F}_n yields, for $n \geq 1$,

$$\begin{aligned}
\mathbb{E}[V(\Sigma_{n+1})|\mathcal{F}_n] &\leq V(\Sigma_n) + \mathbb{E}[\Delta t_n \text{tr}((\mathbf{L}_n^T \mathbf{L}_n - I)(-\mathbf{L}_n^T \mathbf{L}_n + I))|\mathcal{F}_n] + \mathbb{E}[\Delta t_n \text{tr}((\mathbf{L}_n^T \mathbf{L}_n - I)\Omega_n)|\mathcal{F}_n] \\
&\quad + \mathbb{E}[(\Delta t_n)^2 \text{tr}(\mathbf{L}_n^T \mathbf{L}_n(-\mathbf{L}_n^T \mathbf{L}_n + I + \Omega_n)^2)|\mathcal{F}_n] \\
&= V(\Sigma_n) - \left(\mathbb{E}[\Delta t_n \|\Sigma_n - I\|_F^2|\mathcal{F}_n] - \min\{\mathbb{E}[\Delta t_n \text{tr}((\mathbf{L}_n^T \mathbf{L}_n - I)\Omega_n)|\mathcal{F}_n], 0\} \right) \\
&\quad + \underbrace{\mathbb{E}[(\Delta t_n)^2 \text{tr}(\mathbf{L}_n^T \mathbf{L}_n(-\mathbf{L}_n^T \mathbf{L}_n + I + \Omega_n)^2)|\mathcal{F}_n]}_{Z_n^{(1)}} + \underbrace{\max\{\mathbb{E}[\Delta t_n \text{tr}((\mathbf{L}_n^T \mathbf{L}_n - I)\Omega_n)|\mathcal{F}_n], 0\}}_{Z_n^{(2)}}.
\end{aligned}$$

By the boundness of \mathbf{L}_n from [Assumption 1](#) and the tail bound in (A.12), there exists $C_4 > 0$ such that $\mathbb{E}[\text{tr}(\mathbf{L}_n^T \mathbf{L}_n(-\mathbf{L}_n^T \mathbf{L}_n + I + \Omega_n)^2)|\mathcal{F}_n] < C_4$ and $\mathbb{E}[|\text{tr}((\mathbf{L}_n^T \mathbf{L}_n - I)\Omega_n)|^2|\mathcal{F}_n] < C_4$ for all n . Since $\text{tr}(\mathbf{L}_n^T \mathbf{L}_n(-\mathbf{L}_n^T \mathbf{L}_n + I + \Omega_n)^2) \geq 0$, we have

$$\sum_{n=1}^{\infty} Z_n^{(1)} \leq \sum_{n=1}^{\infty} (\eta(t_n) \Delta t_{\max})^2 \mathbb{E}[\text{tr}(\mathbf{L}_n^T \mathbf{L}_n(-\mathbf{L}_n^T \mathbf{L}_n + I + \Omega_n)^2)|\mathcal{F}_n] \leq \sum_{n=1}^{\infty} (\eta(t_n) \Delta t_{\max})^2 C_4 < \infty.$$

From [Assumption 1](#) the noise Ω_n has zero mean, i.e., $\mathbb{E}[\Omega_n|\mathcal{F}_n] = 0$, and thus

$$\begin{aligned}
\sum_{n=1}^{\infty} Z_n^{(2)} &= \sum_{n=1}^{\infty} \max\{\mathbb{E}[(\Delta t_n - \Delta t_{\max} \eta(t_n)) \text{tr}((\mathbf{L}_n^T \mathbf{L}_n - I)\Omega_n)|\mathcal{F}_n], 0\} \\
&= \sum_{n=1}^{\infty} \max\{\mathbb{E}[(\Delta t_n - \Delta t_{\max} \eta(t_n)) \mathbf{1}_{A_n} \text{tr}((\mathbf{L}_n^T \mathbf{L}_n - I)\Omega_n)|\mathcal{F}_n], 0\} \\
&\leq \sum_{n=1}^{\infty} 2 \Delta t_{\max} \eta(t_n) \sqrt{\mathbb{E}[\mathbf{1}_{A_n}|\mathcal{F}_n]} \sqrt{\mathbb{E}[|\text{tr}((\mathbf{L}_n^T \mathbf{L}_n - I)\Omega_n)|^2|\mathcal{F}_n]} \\
&\leq 2 \Delta t_{\max} \sqrt{C_4} \sum_{n=1}^{\infty} \eta(t_n) \sqrt{\mathbb{E}[\mathbf{1}_{A_n}|\mathcal{F}_n]} < \infty,
\end{aligned}$$

where in the last inequality we used $\mathbb{E}[\mathbf{1}_{A_n}|\mathcal{F}_n] = \mathbb{P}(A_n|\mathcal{F}_n) \lesssim \eta(t_n)^2$ from (A.13). Applying the Robbins-Siegmund theorem [53] to (A.17), we have $\{V(\Sigma_n)\}_{n \geq 1}$ converges almost surely to a random variable V_{∞} and $\sum_{n=1}^{\infty} \mathbb{E}[\Delta t_n \|\Sigma_n - I\|_F^2|\mathcal{F}_n] - \min\{\mathbb{E}[\Delta t_n \text{tr}((\mathbf{L}_n^T \mathbf{L}_n - I)\Omega_n)|\mathcal{F}_n], 0\} < \infty$ almost surely. Since $\mathbb{E}[\Delta t_n \|\Sigma_n - I\|_F^2|\mathcal{F}_n] = \mathbb{E}[\Delta t_n \mathbf{1}_{A_n} \|\Sigma_n - I\|_F^2|\mathcal{F}_n] + \mathbb{E}[\Delta t_n \mathbf{1}_{A_n^c} \|\Sigma_n - I\|_F^2|\mathcal{F}_n]$, we have almost surely that $\sum_{n=1}^{\infty} \mathbb{E}[\Delta t_n \mathbf{1}_{A_n^c} \|\Sigma_n - I\|_F^2|\mathcal{F}_n] = \sum_{n=1}^{\infty} \Delta t_{\max} \eta(t_n) (1 - \mathbb{P}(A_n)) \|\Sigma_n - I\|_F^2 < \infty$. Since $\sum_{n=1}^{\infty} \eta(t_n) = \infty$ and $\sum_{n=1}^{\infty} \mathbb{P}(A_n) < \infty$, it follows that $\liminf_{n \rightarrow \infty} \|\Sigma_n - I\|_F^2 = 0$ almost surely. Combined with the almost sure convergence of $V(\Sigma_n)$, this implies $V(\Sigma_n) \xrightarrow{\text{a.s.}} 0$, and hence $\Sigma_n \xrightarrow{\text{a.s.}} I$.

Step 4. v_n converges to 0 almost surely. We compute

$$\|v_{n+1}\|_2^2 = \|v_n - \Delta t_n (\mathbf{L}_n (\mathbf{L}_n^T v_n + \tilde{w}_n))\|_2^2 = \|v_n\|_2^2 - 2\Delta t_n v_n^T (\mathbf{L}_n (\mathbf{L}_n^T v_n + \tilde{w}_n)) + \Delta t_n^2 \|\mathbf{L}_n (\mathbf{L}_n^T v_n + \tilde{w}_n)\|_2^2.$$

Taking conditional expectations with respect to the filtration \mathcal{F}_n yields, for $n \geq 1$,

$$\begin{aligned}
\mathbb{E}[\|v_{n+1}\|_2^2|\mathcal{F}_n] &\leq \|v_n\|_2^2 - \mathbb{E}[2\Delta t_n (v_n^T \Sigma_n v_n + v_n^T \mathbf{L}_n \tilde{w}_n)|\mathcal{F}_n] + \mathbb{E}[\Delta t_n^2 \|\mathbf{L}_n (\mathbf{L}_n^T v_n + \tilde{w}_n)\|_2^2|\mathcal{F}_n] \\
(A.18) \quad &= \|v_n\|_2^2 - (\mathbb{E}[2\Delta t_n v_n^T \Sigma_n v_n|\mathcal{F}_n] + \max\{\mathbb{E}[2\Delta t_n v_n^T \mathbf{L}_n \tilde{w}_n|\mathcal{F}_n], 0\}) \\
&\quad + \mathbb{E}[\Delta t_n^2 \|\mathbf{L}_n (\mathbf{L}_n^T v_n + \tilde{w}_n)\|_2^2|\mathcal{F}_n] - \min\{\mathbb{E}[2\Delta t_n v_n^T \mathbf{L}_n \tilde{w}_n|\mathcal{F}_n], 0\}.
\end{aligned}$$

By the boundedness of L_n and v_n , from [Assumption 1](#) and the tail bound in [\(A.12\)](#), there exists $C_5 > 0$ such that $\mathbb{E}[\Delta t_n^2 \|L_n(L_n^T v_n + \tilde{w}_n)\|_2^2 | \mathcal{F}_n] \leq \Delta t_{\max}^2 \eta(t_n)^2 \mathbb{E}[2\|L_n\|_2^2 (\|L_n\|_2^2 \|v_n\|_2^2 + \|\tilde{w}_n\|_2^2) | \mathcal{F}_n] \leq C_5 \eta(t_n)^2$, and $\mathbb{E}[(v_n^T L_n \tilde{w}_n)^2 | \mathcal{F}_n] \leq C_5$. We have

$$\begin{aligned} \sum_{n=1}^{\infty} \mathbb{E}[\Delta t_n^2 \|L_n(L_n^T v_n + \tilde{w}_n)\|_2^2 | \mathcal{F}_n] &\leq \sum_{n=1}^{\infty} C_5 \eta(t_n)^2 < \infty, \\ \sum_{n=1}^{\infty} -\min\{\mathbb{E}[2\Delta t_n v_n^T L_n \tilde{w}_n | \mathcal{F}_n], 0\} &= \sum_{n=1}^{\infty} -\min\{\mathbb{E}[2(\Delta t_n - \Delta t_{\max} \eta(t_n)) v_n^T L_n \tilde{w}_n | \mathcal{F}_n], 0\} \\ &= \sum_{n=1}^{\infty} -\min\{\mathbb{E}[2(\Delta t_n - \Delta t_{\max} \eta(t_n)) 1_{A_n} v_n^T L_n \tilde{w}_n | \mathcal{F}_n], 0\} \\ &\leq \sum_{n=1}^{\infty} 4\Delta t_{\max} \eta(t_n) \sqrt{\mathbb{E}[1_{A_n} | \mathcal{F}_n]} \sqrt{\mathbb{E}[(v_n^T L_n \tilde{w}_n)^2 | \mathcal{F}_n]} \\ &\leq \sum_{n=1}^{\infty} 4\Delta t_{\max} \eta(t_n) \sqrt{\mathbb{P}(A_n | \mathcal{F}_n)} \sqrt{C_5} < \infty. \end{aligned} \quad \square$$

In the second equation, we used that $\mathbb{E}[\tilde{w}_n | \mathcal{F}_n] = 0$ and $\mathbb{P}(A_n | \mathcal{F}_n) \lesssim \eta(t_n)^2$ in [\(A.13\)](#). Applying the Robbins-Siegmund theorem [\[53\]](#) to [\(A.18\)](#) we have that $\{v_n\}_{n \geq 1}$ converges almost surely to a random variable v_{∞} and that $\sum_{n=1}^{\infty} (\mathbb{E}[2\Delta t_n v_n^T \Sigma_n v_n | \mathcal{F}_n] + \max\{\mathbb{E}[2\Delta t_n L_n \tilde{w}_n | \mathcal{F}_n], 0\}) < \infty$ almost surely. Since $\mathbb{E}[2\Delta t_n v_n^T \Sigma_n v_n | \mathcal{F}_n] \geq \mathbb{E}[2\Delta t_n 1_{A_n} v_n^T \Sigma_n v_n | \mathcal{F}_n]$, we have almost surely that $\sum_{n=1}^{\infty} \mathbb{E}[2\Delta t_n 1_{A_n} v_n^T \Sigma_n v_n | \mathcal{F}_n] = \sum_{n=1}^{\infty} 2\Delta t_{\max} \eta(t_n) (1 - \mathbb{P}(A_n)) v_n^T \Sigma_n v_n < \infty$. Since $\sum_{n=1}^{\infty} \eta(t_n) = \infty$, $\sum_{n=1}^{\infty} \mathbb{P}(A_n) < \infty$, and $\Sigma_n \xrightarrow{\text{a.s.}} I$, it follows that $\liminf_{n \rightarrow \infty} \|v_n\|_2^2 = 0$ almost surely. Combined with the almost sure convergence of $\|v_n\|_2^2$, this implies $\|v_n\|_2^2 \xrightarrow{\text{a.s.}} 0$, and hence $v_n \xrightarrow{\text{a.s.}} 0$.

Appendix B. Proof of the Manifold Optimization.

LEMMA B.1. *For every square-root factorization $X = LL^T$, we have*

$$\begin{aligned} d(X, Y) &= \|\log(L^{-1}YL^{-T})\|_F, \\ \exp_X(\sigma) &= L \exp(L^{-1}\sigma L^{-T})L^T, \\ \exp_X^{-1}(Y) &= L \log(L^{-1}YL^{-T})L^T. \end{aligned}$$

Proof. As $(X^{\frac{1}{2}}L^{-T})(X^{\frac{1}{2}}L^{-T})^T = X^{\frac{1}{2}}L^{-T}L^{-1}X^{\frac{1}{2}} = I$, $X^{\frac{1}{2}}L^{-T}$ is orthogonal. Using this property and the identity $X^{\frac{1}{2}}L^{-T} = (L^{-1}X^{\frac{1}{2}})^{-1} = X^{-\frac{1}{2}}L$, we have

$$\begin{aligned} \|\log(X^{-\frac{1}{2}}YX^{-\frac{1}{2}})\|_F &= \|(X^{\frac{1}{2}}L^{-T})^T \log(X^{-\frac{1}{2}}YX^{-\frac{1}{2}})(X^{\frac{1}{2}}L^{-T})\|_F \\ &= \left\| \log \left((X^{\frac{1}{2}}L^{-T})^T X^{-\frac{1}{2}}YX^{-\frac{1}{2}} (X^{\frac{1}{2}}L^{-T}) \right) \right\|_F \\ &= \|\log(L^{-1}YL^{-T})\|_F, \\ X^{\frac{1}{2}} \exp(X^{-\frac{1}{2}}\sigma X^{-\frac{1}{2}})X^{\frac{1}{2}} &= X^{\frac{1}{2}} \exp(X^{-\frac{1}{2}}LL^{-1}\sigma L^{-T}L^T X^{-\frac{1}{2}})X^{\frac{1}{2}} \\ &= X^{\frac{1}{2}} X^{-\frac{1}{2}} L \exp(L^{-1}\sigma L^{-T}) L^T X^{-\frac{1}{2}} X^{\frac{1}{2}} \\ &= L \exp(L^{-1}\sigma L^{-T}) L^T, \\ X^{\frac{1}{2}} \log(X^{-\frac{1}{2}}YX^{-\frac{1}{2}})X^{\frac{1}{2}} &= X^{\frac{1}{2}} \log(X^{-\frac{1}{2}}LL^{-1}YL^{-T}L^T X^{-\frac{1}{2}})X^{\frac{1}{2}} \\ &= X^{\frac{1}{2}} X^{-\frac{1}{2}} L \log(L^{-1}YL^{-T}) L^T X^{-\frac{1}{2}} X^{\frac{1}{2}} \\ &= L \log(L^{-1}YL^{-T}) L^T. \end{aligned} \quad \square$$

Proof of Theorem 3.5. We first prove the mirror descent (3.8) is consistent with our update (2.5) (2.6). By the construction of our algorithm, we only need to prove

$$(B.1) \quad C_{k,n+1} = \exp_{C_{k,n}} \left(-\frac{2\Delta t_n}{w_{k,n}} g_{C_{k,n}} \right),$$

$$(B.2) \quad m_{k,n+1} = m_{k,n} - \Delta t_n \frac{C_{k,n}}{w_{k,n}} g_{m_{k,n}},$$

$$(B.3) \quad w_{k,n+1} = \frac{w_{k,n} \exp(-\Delta t_n g_{w_{k,n}})}{\sum_{j=1}^K w_{j,n} \exp(-\Delta t_n g_{w_{j,n}})},$$

where $g_{C_{k,n}} = \text{grad}_{C_k} \text{KL}[\rho_a^{\text{GM}} \|\pi]|_{C_{k,n}}$, $g_{m_{k,n}} = \nabla_{m_k} \text{KL}[\rho_a^{\text{GM}} \|\pi]|_{m_{k,n}}$, $g_{w_{k,n}} = \nabla_{w_k} \text{KL}[\rho_a^{\text{GM}} \|\pi]|_{w_{k,n}}$. \blacksquare

Note that the mirror descent (3.8) can decompose as a sum over k components involving the partial gradients with respect to m_k , C_k , w_k , and each component can be divided into covariance, mean, and weight terms, which can be analyzed separately.

For the covariance term, let $f(C_k) = \text{tr}(S_{k,n} \log S_{k,n} - S_{k,n})$, $S_{k,n} = C_{k,n}^{-\frac{1}{2}} C_k C_{k,n}^{-\frac{1}{2}}$. Then $\nabla f(C_k) = C_{k,n}^{-1} \exp_{C_{k,n}}^{-1}(C_k) C_{k,n}^{-1}$ and $\nabla f(C_k)|_{C_{k,n}} = 0$. Therefore, we have

$$C_{k,n+1} = \underset{C_k}{\text{argmin}} \left\{ \langle C_{k,n}^{-1} g_{C_{k,n}} C_{k,n}^{-1}, C_k - C_{k,n} \rangle + \frac{w_{k,n}}{2\Delta t_n} f(C_k) \right\},$$

By the first-order optimality condition,

$$C_{k,n}^{-1} g_{C_{k,n}} C_{k,n}^{-1} + \frac{w_{k,n}}{2\Delta t_n} C_{k,n}^{-1} \exp_{C_{k,n}}^{-1}(C_{k,n+1}) C_{k,n}^{-1} = 0,$$

which means $C_{k,n+1} = \exp_{C_{k,n}} \left(-\frac{2\Delta t_n}{w_{k,n}} g_{C_{k,n}} \right)$. For the mean term,

$$m_{k,n+1} = \underset{m}{\text{argmin}} \left\{ \langle m - m_{k,n}, g_{m_{k,n}} \rangle + \frac{w_{k,n}}{2\Delta t_n} (m - m_{k,n})^T C_{k,n}^{-1} (m - m_{k,n}) \right\},$$

this directly yields (B.2). For the weight term, define $\text{KL}(w, w_n) = \sum_{k=1}^K w_k (\log w_k - \log w_{k,n})$, we have

$$w_{n+1} = \underset{w}{\text{argmin}} \left\{ \langle w - w_n, [g_{w_{1,n}}, \dots, g_{w_{K,n}}]^T \rangle + \frac{1}{\Delta t_n} \text{KL}(w, w_n) \right\} \quad \text{s.t.} \quad w^T \mathbf{1} = 1,$$

which directly yields (B.3).

Next, we prove the affine invariance property of our algorithm at the discrete level. Consider an arbitrary invertible affine transformation $\psi: \theta \mapsto \tilde{\theta} = T\theta + d$. In the transformed coordinate system, the parameters are

$$\tilde{m}_k(t_n) = Tm_k(t_n) + d, \quad \tilde{L}_k(t_n) = TL_k(t_n), \quad \tilde{C}_k(t_n) = \tilde{L}_k(t_n) \tilde{L}_k(t_n)^T = TC_k(t_n)T^T. \blacksquare$$

The function to be estimated in the new coordinates is defined by

$$\begin{aligned} \tilde{f}_k(\theta) &= \log \rho_a^{\text{GM}}(\tilde{m}_k + \tilde{L}_k \theta) + \tilde{\Phi}_R(\tilde{m}_k + \tilde{L}_k \theta) \\ &= \log \left(|\det T|^{-1} \rho_a^{\text{GM}}(T^{-1}(\tilde{m}_k + \tilde{L}_k \theta - d)) \right) + \Phi_R(T^{-1}(\tilde{m}_k + \tilde{L}_k \theta - d)) \\ &= -\log |\det T| + \log \rho_a^{\text{GM}}(m_k + L_k \theta) + \Phi_R(m_k + L_k \theta) \\ &= f_k(\theta) - \log |\det T|. \end{aligned}$$

This relation immediately implies

$$\tilde{E}_k(t) = \mathbb{E}_{\mathcal{N}} \left[\theta \theta^T (\tilde{f}_k(t, \theta) - \mathbb{E}_{\mathcal{N}}[\tilde{f}_k(t, \theta)]) \right] = \mathbb{E}_{\mathcal{N}} \left[\theta \theta^T (f_k(t, \theta) - \mathbb{E}_{\mathcal{N}}[f_k(t, \theta)]) \right] = E_k(t). \blacksquare$$

Consequently, the adaptive step size remains unchanged:

$$\Delta \tilde{t}_n = \min \left\{ \Delta t_{\max} \eta(t_n), \frac{\beta}{\max_k \{\|\tilde{E}_k(t_n)\|_2\}} \right\} = \Delta t_n.$$

We now verify the affine invariance of each update. For the covariance update, we have

$$\begin{aligned} \tilde{C}_k(t_n + \Delta t_n) &= \tilde{L}_k(t_n) e^{-\tilde{E}_k(t_n) \Delta t_n} \tilde{L}_k(t_n)^T \\ &= (T L_k(t_n)) e^{-E_k(t_n) \Delta t_n} (T L_k(t_n))^T \\ &= T C_k(t_n + \Delta t_n) T^T. \end{aligned}$$

For the mean update, we have

$$\begin{aligned} \tilde{m}_k(t_n + \Delta t_n) &= \tilde{m}_k(t_n) - \Delta t_n \tilde{L}_k(t_n + \Delta t_n) \mathbb{E}_{\mathcal{N}} \left[\theta (\tilde{f}_k(t_n, \theta) - \mathbb{E}_{\mathcal{N}}[\tilde{f}_k(t_n, \theta)]) \right] \\ &= (T m_k(t_n) + d) - \Delta t_n (T L_k(t_n)) \mathbb{E}_{\mathcal{N}} \left[\theta (f_k(t_n, \theta) - \mathbb{E}_{\mathcal{N}}[f_k(t_n, \theta)]) \right] \\ &= T m_k(t_n + \Delta t_n) + d. \end{aligned}$$

For the weight update, we have

$$\begin{aligned} \log \tilde{w}_k(t_n + \Delta t_n) &= \log \tilde{w}_k(t_n) - \Delta t_n \left(\mathbb{E}_{\mathcal{N}}[\tilde{f}_k(t_n, \theta)] - \sum_i \tilde{w}_i(t_n) \mathbb{E}_{\mathcal{N}}[\tilde{f}_i(t_n, \theta)] \right) \\ &= \log w_k(t_n) - \Delta t_n \left(\mathbb{E}_{\mathcal{N}}[f_k(t_n, \theta)] - \sum_i w_i(t_n) \mathbb{E}_{\mathcal{N}}[f_i(t_n, \theta)] \right) \\ &= \log w_k(t_n + \Delta t_n). \end{aligned}$$

In all cases, the transformed parameters after one update step coincide with the affine transformation of the original updated parameters. This establishes the affine invariance of the complete update scheme. \square

Appendix C. Sensitivity study. In this section, we study the sensitivity of GMBBVI to the initial conditions, the number of modes K , the scheduler η , and the annealing strategy in the 10-dimensional Case A. For the initial conditions, we shift the initial mode means by ± 2 in all components prior to annealing. For the number of modes, we consider $K = 10, 20, 40$. For the scheduler, we evaluate three schedulers: stable cosine decay (4.1), stable linear decay (replacing the cosine decay phase with a linear decay phase), and exponential decay. Finally, we study three annealing strategies: no annealing, annealing with $N_\alpha = 500$ and $\alpha = 0.5$, and annealing with $N_\alpha = 500$ and $\alpha = 0.1$. The resulting densities after 500 iteration are shown in Figure 7 indicating that GMBBVI is robust with respect to the initial condition, the scheduler, the annealing parameter (with annealing being essential), and the number of modes. In particular, when $K = 10$, GMBBVI may miss some of the target modes, but for $K = 20, 40$, all target modes are accurately recovered.

REFERENCES

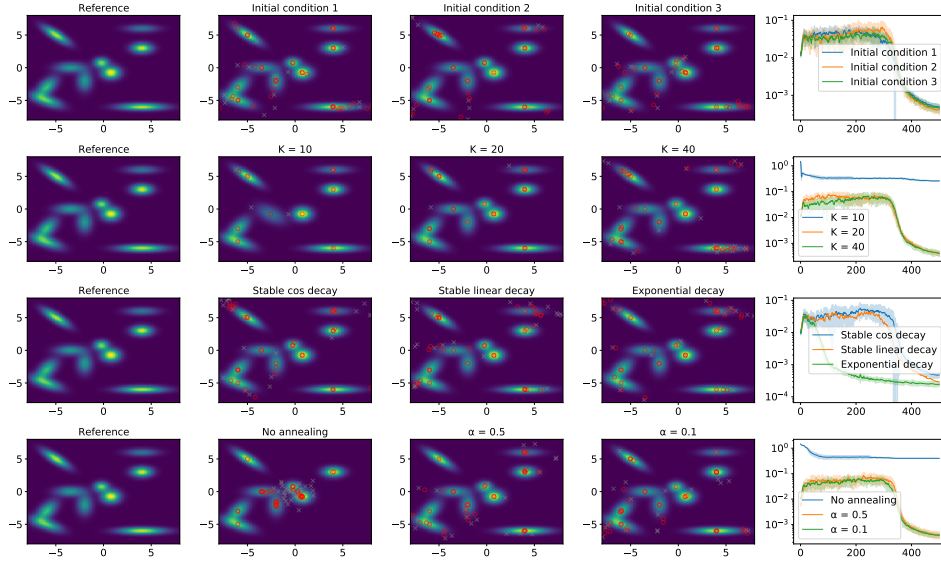


Fig. 7: Sensitivity study for different choices of initial condition (first row), number of modes K (second row), scheduler η (third row) and annealing strategy (last row) in the 10-dimensional Case A. The fifth panel reports the TV distance between the reference marginal density and the estimated marginal densities across iterations, where solid line represents the mean, and shaded area represents the standard deviation computed from 10 independent trials.

- [1] S.-I. AMARI, *Natural gradient works efficiently in learning*, Neural computation, 10 (1998), pp. 251–276.
- [2] I. ARASARATNAM AND S. HAYKIN, *Cubature Kalman filters*, IEEE Transactions on automatic control, 54 (2009), pp. 1254–1269.
- [3] H. ATTIAS, *Inferring parameters and structure of latent variable models by variational bayes*, 2013, <https://arxiv.org/abs/1301.6676>.
- [4] A. BECK AND M. TEBOULLE, *Mirror descent and nonlinear projected subgradient methods for convex optimization*, Operations Research Letters, 31 (2003), pp. 167–175.
- [5] C. M. BISHOP AND N. M. NASRABADI, *Pattern recognition and machine learning*, vol. 4, Springer, 2006.
- [6] D. M. BLEI, A. KUCUKELBIR, AND J. D. McAULIFFE, *Variational inference: A review for statisticians*, Journal of the American statistical Association, 112 (2017), pp. 859–877.
- [7] T. BUI-THANH, O. GHATTAS, J. MARTIN, AND G. STADLER, *A computational framework for infinite-dimensional Bayesian inverse problems. Part I: The linearized case, with application to global seismic inversion*, SIAM Journal on Scientific Computing, 35 (2013), pp. A2494–A2523.
- [8] M. BURGER, M. ERBAR, F. HOFFMANN, D. MATTIES, AND A. SCHLICHTING, *Covariance-modulated optimal transport and gradient flows*, Archive for Rational Mechanics and Analysis, 249 (2025), p. 7.
- [9] S. CAO AND D. ZHENGYU HUANG, *Bayesian calibration for large-scale fluid structure interaction problems under embedded/immersed boundary framework*, International Journal for Numerical Methods in Engineering, 123 (2022), pp. 1791–1812.
- [10] J. CARRILLO AND U. VAES, *Wasserstein stability estimates for covariance-preconditioned fokker-planck equations*, Nonlinearity, 34 (2021), p. 2275.
- [11] J. A. CARRILLO, Y. CHEN, D. Z. HUANG, J. HUANG, AND D. WEI, *Fisher-rao gradient flow: geodesic convexity and functional inequalities*, arXiv preprint arXiv:2407.15693, (2024).
- [12] N. K. CHADA, A. M. STUART, AND X. T. TONG, *Tikhonov regularization within ensemble Kalman inversion*, SIAM Journal on Numerical Analysis, 58 (2020), pp. 1263–1294.

- [13] B. CHE, Y. CHEN, Z. HUAN, D. Z. HUANG, AND W. WANG, *Stable derivative free gaussian mixture variational inference for bayesian inverse problems*, SIAM Journal on Scientific Computing, 47 (2025), pp. A2583–A2608, <https://doi.org/10.1137/25M1722548>.
- [14] S. CHEN, Q. LI, O. TSE, AND S. J. WRIGHT, *Accelerating optimization over the space of probability measures*, Journal of machine learning research, 26 (2025), pp. 1–40.
- [15] Y. CHEN, D. Z. HUANG, J. HUANG, S. REICH, AND A. M. STUART, *Gradient flows for sampling: Mean-field models, Gaussian approximations and affine invariance*, arXiv preprint arXiv:2302.11024, (2023).
- [16] Y. CHEN, D. Z. HUANG, J. HUANG, S. REICH, AND A. M. STUART, *Sampling via gradient flows in the space of probability measures*, arXiv preprint arXiv:2310.03597, (2023).
- [17] Y. CHEN, D. Z. HUANG, J. HUANG, S. REICH, AND A. M. STUART, *Efficient, multimodal, and derivative-free bayesian inference with fisher-rao gradient flows*, Inverse Problems, 40 (2024), p. 125001.
- [18] Y. CHEN AND S. LIU, *Rotated mean-field variational inference and iterative gaussianization*, arXiv preprint arXiv:2510.07732, (2025).
- [19] T. CUI, Y. M. MARZOUK, AND K. E. WILLCOX, *Data-driven model reduction for the bayesian solution of inverse problems*, International Journal for Numerical Methods in Engineering, 102 (2015), pp. 966–990.
- [20] J. DOMKE, R. GOWER, AND G. GARRIGOS, *Provable convergence guarantees for black-box variational inference*, Advances in neural information processing systems, 36 (2023), pp. 66289–66327.
- [21] G. EVENSEN, *Sequential data assimilation with a nonlinear quasi-geostrophic model using Monte Carlo methods to forecast error statistics*, Journal of Geophysical Research: Oceans, 99 (1994), pp. 10143–10162.
- [22] A. GARBUNO-INIGO, F. HOFFMANN, W. LI, AND A. M. STUART, *Interacting Langevin diffusions: Gradient structure and ensemble Kalman sampler*, SIAM Journal on Applied Dynamical Systems, 19 (2020), pp. 412–441.
- [23] A. GARBUNO-INIGO, N. NÜSKEN, AND S. REICH, *Affine invariant interacting Langevin dynamics for Bayesian inference*, SIAM Journal on Applied Dynamical Systems, 19 (2020), pp. 1633–1658.
- [24] S. GERSHMAN, M. HOFFMAN, AND D. BLEI, *Nonparametric variational inference*, arXiv preprint arXiv:1206.4665, (2012).
- [25] J. GOODMAN AND J. WEARE, *Ensemble samplers with affine invariance*, Communications in applied mathematics and computational science, 5 (2010), pp. 65–80.
- [26] L. GUO, H. WU, Y. WANG, W. ZHOU, AND T. ZHOU, *Ib-uq: Information bottleneck based uncertainty quantification for neural function regression and neural operator learning*, Journal of Computational Physics, 510 (2024), p. 113089.
- [27] A. HAN, B. MISHRA, P. K. JAWANPURIA, AND J. GAO, *On riemannian optimization over positive definite matrices with the bures-wasserstein geometry*, Advances in Neural Information Processing Systems, 34 (2021), pp. 8940–8953.
- [28] J. HAN AND Q. LIU, *Stein variational gradient descent without gradient*, in International Conference on Machine Learning, PMLR, 2018, pp. 1900–1908.
- [29] S. HENNEKING, S. VENKAT, V. DOBREV, J. CAMIER, T. KOLEV, M. FERNANDO, A.-A. GABRIEL, AND O. GHATTAS, *Real-time bayesian inference at extreme scale: A digital twin for tsunami early warning applied to the cascadia subduction zone*, in Proceedings of the International Conference for High Performance Computing, Networking, Storage and Analysis, 2025, pp. 60–71.
- [30] M. HOFFMAN, D. M. BLEI, C. WANG, AND J. PAISLEY, *Stochastic variational inference*, 2013, <https://arxiv.org/abs/1206.7051>.
- [31] M. D. HOFFMAN, A. GELMAN, ET AL., *The no-u-turn sampler: adaptively setting path lengths in hamiltonian monte carlo*, J. Mach. Learn. Res., 15 (2014), pp. 1593–1623.
- [32] D. Z. HUANG, J. HUANG, S. REICH, AND A. M. STUART, *Efficient derivative-free bayesian inference for large-scale inverse problems*, arXiv preprint arXiv:2204.04386, (2022).
- [33] D. Z. HUANG, T. SCHNEIDER, AND A. M. STUART, *Iterated kalman methodology for inverse problems*, Journal of Computational Physics, (2022), p. 111262.
- [34] T. S. JAAKKOLA AND M. I. JORDAN, *Improving the mean field approximation via the use of mixture distributions*, in Learning in graphical models, Springer, 1998, pp. 163–173.
- [35] M. I. JORDAN, Z. GHAHRAMANI, T. S. JAAKKOLA, AND L. K. SAUL, *An introduction to variational methods for graphical models*, Machine learning, 37 (1999), pp. 183–233.
- [36] S. J. JULIER, J. K. UHLMANN, AND H. F. DURRANT-WHYTE, *A new approach for filtering nonlinear systems*, in Proceedings of 1995 American Control Conference-ACC'95, vol. 3, IEEE, 1995, pp. 1628–1632.

- [37] J. KAIPIO AND E. SOMERSALO, *Statistical and computational inverse problems*, vol. 160, Springer Science & Business Media, 2006.
- [38] R. E. KALMAN, *A new approach to linear filtering and prediction problems*, J. Basic Eng. Mar, 82 (1960), pp. 35–45.
- [39] M. LAMBERT, S. CHEWI, F. BACH, S. BONNABEL, AND P. RIGOLLET, *Variational inference via wasserstein gradient flows*, arXiv preprint arXiv:2205.15902, (2022).
- [40] B. LI, F. CHEN, Z. HUANG, L. WANG, AND L. WU, *Functional scaling laws in kernel regression: Loss dynamics and learning rate schedules*, arXiv preprint arXiv:2509.19189, (2025).
- [41] W. LIN, M. E. KHAN, AND M. SCHMIDT, *Fast and simple natural-gradient variational inference with mixture of exponential-family approximations*, in International Conference on Machine Learning, PMLR, 2019, pp. 3992–4002.
- [42] S. LIU, S. REICH, AND X. T. TONG, *Dropout ensemble kalman inversion for high dimensional inverse problems*, SIAM Journal on Numerical Analysis, 63 (2025), pp. 685–715.
- [43] I. LOSHCHELOV AND F. HUTTER, *Sgdr: Stochastic gradient descent with warm restarts*, arXiv preprint arXiv:1608.03983, (2016).
- [44] J. MARTENS, *New insights and perspectives on the natural gradient method*, The Journal of Machine Learning Research, 21 (2020), pp. 5776–5851.
- [45] T. S. K. NAWAF BOU-RABEE, BOB CARPENTER AND S. LIU, *The within-orbit adaptive leapfrog no-u-turn sampler*, arXiv preprint arXiv:2506.18746, (2025).
- [46] R. M. NEAL, *Slice sampling*, The annals of statistics, 31 (2003), pp. 705–767.
- [47] D. S. OLIVER, A. C. REYNOLDS, AND N. LIU, *Inverse theory for petroleum reservoir characterization and history matching*, Cambridge University Press, 2008.
- [48] M. OPPER AND C. ARCHAMBEAU, *The variational Gaussian approximation revisited*, Neural computation, 21 (2009), pp. 786–792.
- [49] J. PAISLEY, D. BLEI, AND M. JORDAN, *Variational bayesian inference with stochastic search*, arXiv preprint arXiv:1206.6430, (2012).
- [50] X. PENNEC, P. FILLARD, AND N. AYACHE, *A riemannian framework for tensor computing*, International Journal of computer vision, 66 (2006), pp. 41–66.
- [51] R. RANGANATH, S. GERRISH, AND D. BLEI, *Black box variational inference*, in Artificial intelligence and statistics, PMLR, 2014, pp. 814–822.
- [52] D. REZENDE AND S. MOHAMED, *Variational inference with normalizing flows*, in International conference on machine learning, PMLR, 2015, pp. 1530–1538.
- [53] H. ROBBINS AND D. SIEGMUND, *A convergence theorem for non negative almost supermartingales and some applications*, in Optimizing Methods in Statistics, J. S. Rustagi, ed., Academic Press, 1971, pp. 233–257, <https://doi.org/10.1016/B978-0-12-604550-5.50015-8>.
- [54] G. ROEDER, Y. WU, AND D. K. DUVENAUD, *Sticking the landing: Simple, lower-variance gradient estimators for variational inference*, Advances in Neural Information Processing Systems, 30 (2017).
- [55] C. SCHILLINGS AND C. SCHWAB, *Sparse, adaptive smolyak quadratures for bayesian inverse problems*, Inverse Problems, 29 (2013), p. 065011.
- [56] A. M. STUART, *Inverse problems: A Bayesian perspective*, Acta numerica, 19 (2010), pp. 451–559.
- [57] M. WELANDAWE, M. R. ANDERSEN, A. VEHTARI, AND J. H. HUGGINS, *A framework for improving the reliability of black-box variational inference*, Journal of Machine Learning Research, 25 (2024), pp. 1–71, <http://jmlr.org/papers/v25/22-0327.html>.
- [58] L. YAN AND T. ZHOU, *An adaptive surrogate modeling based on deep neural networks for large-scale bayesian inverse problems*, Communications in Computational Physics, 28 (2020), pp. 2180–2205, <https://doi.org/10.4208/cicp.OA-2020-0186>.